


January 2013

Structural Basis for Ternary Complex Formation Between tau, Hsp90, and FKBP51

Alexander Steven Barrett

University of South Florida, asbarrett@mail.usf.edu

Follow this and additional works at: <http://scholarcommons.usf.edu/etd>

 Part of the [Biochemistry Commons](#), [Biophysics Commons](#), and the [Molecular Biology Commons](#)

Scholar Commons Citation

Barrett, Alexander Steven, "Structural Basis for Ternary Complex Formation Between tau, Hsp90, and FKBP51" (2013). *Graduate Theses and Dissertations*.

<http://scholarcommons.usf.edu/etd/4436>

This Thesis is brought to you for free and open access by the Graduate School at Scholar Commons. It has been accepted for inclusion in Graduate Theses and Dissertations by an authorized administrator of Scholar Commons. For more information, please contact scholarcommons@usf.edu.

Structural Basis for Ternary Complex Formation Between tau, Hsp90, and
FKBP51

by

Alexander S. Barrett

A thesis submitted in partial fulfillment of
the requirements for the degree of
Master of Science
Department of Cell Biology, Microbiology, and Molecular Biology
College of Arts and Sciences,
University of South Florida

Major Professor: Gary Daughdrill, Ph.D.
Stanley Stevens, Ph.D.
Sameer Varma, Ph.D.

Date of Approval:
March 25, 2013

Keywords: Nuclear Magnetic Resonance, Tau, Molecular Chaperones
Alzheimer's Disease, Intrinsically Disordered Proteins

Copyright © 2013, Alexander S. Barrett

ACKNOWLEDGMENTS

I would like to acknowledge Dr.'s Bina Nayak and Stepan Kashtanov for their contributions to the tau project. I would also like to acknowledge Bryce Nordheus for his contributions thank him for his insight with experimental protocols. I would like to thank my friend and colleague Wade Borchers for his invaluable support and guidance during my time at the University of South Florida. I would also like to thank my committee members, Dr.'s Stan Stevens and Sameer Varma, for their time and helpful input along the way. Lastly, I would like to thank my major professor, Dr. Gary Daughdrill, for teaching me to focus on the scientific process at hand and not the final product in mind.

TABLE OF CONTENTS

LIST OF TABLES	iii
LIST OF FIGURES	iv
ABSTRACT	vii
CHAPTER ONE: INTRODUCTION	1
Overview of tau biology.....	1
Structure and function of the microtubule associated protein tau	2
Intrinsically disordered proteins in disease	4
The role of molecular chaperones in tau processing	6
FKBP51 is an immunophilin and has PPlase activity.....	8
Structural considerations of the Hsp90 – FKBP51 complex.....	11
Project Summary and Specific Aims.....	12
CHAPTER TWO: PROBING THE NMR STRUCTURE AND DYNAMICS OF TAU AND FKBP51	14
Rationale and Experimental Design.....	14
Sample Preparation of ¹⁵ N-labeled FK1.....	15
3D NMR experiments with ¹³ C ¹⁵ N-labeled FK1	16
Making resonance assignments.....	17
Examining secondary structure in FK1.....	18
2D NMR experiments with ¹⁵ N-labeled FK1.....	19
Characterization of FK1 binding to FK506	20
Characterization of FK1 binding to tau	24
Analysis of resonance intensity ratio plot for ¹⁵ N-labeled FK1	26
CHAPTER THREE: ASSESSING FORMATION OF A TERNARY COMPLEX BETWEEN TAU, HSP90, AND FKBP51 USING NUCLEAR MAGNETIC RESONANCE SPECTROSCOPY	27
Rationale and Experimental Design.....	27
Sample Preparation of 0N4R tau	28

2D NMR experiments with ¹⁵ N-labeled 0N4R tau	30
Assigning 0N4R tau	31
Analysis of resonance intensity ratios	34
N-terminal residues in tau are involved in association with the co- chaperone complex.....	36
Line shape analysis of the most affected resonances in the hexapeptide regions.....	39
Resin binding assay to confirm ternary complex formation.....	41
Model of the Hsp90-FKBP51 complex.....	43
Monitoring the stability of the Hsp90 – FKBP51 complex	45
 CHAPTER FOUR: DISCUSSION	 49
The interaction between the FK1 domain and FK506.....	49
The interaction between the FK1 domain and tau	49
Tau associates with Hsp90 and FKBP51 using two C-terminal hexapeptide motifs.....	50
Possible model of the Hsp90-FKBP51 co-chaperone complex.....	52
 CHAPTER FIVE: MATERIALS AND METHODS.....	 55
Protein expression	55
Protein purification	56
Determining protein concentration	57
NMR data acquisition.....	57
Experimental parameters	57
HSQC and HNCACB experiments	58
Cobalt binding assay.....	59
Molecular dynamics simulation	60
Subcloning of GeneArt constructs	61
Ligation of construct into vector of interest.....	62
Transformation of newly ligated constructs.....	62
Buffer Recipes	63
 LITERATURE CITED	 64
 APPENDICES	 74
Appendix A: Dynamic Light Scattering Results.....	74
Appendix B: NMR Chemical Shift and Assignment Data for FK1	75
Appendix C: NMR Chemical Shift and Assignment Data for tau.....	89
Appendix D: Full length Intensity Ratio Plots for tau Titrations	100

LIST OF TABLES

Table 1: Worktable for restriction digests	61
Table 2: Worktable for ligation reactions	62
Table A1: Peak list and chemical shifts for $^{13}\text{C}^{15}\text{N}$ -labeled FK1	75
Table A2: Secondary C_α chemical shift values	80
Table A3: Intensity ratios for free FK1 vs. FK1 in the presence of tau	85
Table A4: Intensity ratios for ^{15}N -labeled tau titrations.....	89
Table A5: Intensity ratio plot averages and standard deviation values for titrations with ^{15}N -labeled tau.....	99

LIST OF FIGURES

Figure 1: Schematic representation of 0N4R tau.....	3
Figure 2: Schematic representation of alternative of tau	4
Figure 3: IUPRED prediction of 0N4R tau	5
Figure 4: Crystal structure of Hsp90 dimer	8
Figure 5: Domain structure of two FKBP51 monomers	9
Figure 6: Cartoon model of Hsp90 – FKBP51 complex.....	10
Figure 7A: Purification workflow for FK1.....	14
Figure 7B: Purification workflow for FK1.....	15
Figure 8: Neighboring spin systems in FK1 HNCACB spectra	16
Figure 9: Secondary chemical shift values for the PPIase domain of FKBP51	17
Figure 10: $^1\text{H}^{15}\text{N}$ HSQC for free ^{15}N -labeled FK1.....	19
Figure 11: $^1\text{H}^{15}\text{N}$ HSQC for free ^{15}N -labeled FK1 in the presence of FK506	21
Figure 12: Normalized $^1\text{H}^{15}\text{N}$ FK1 chemical shift differences between free FK1 and FK1 bound to natural product FK506	22
Figure 13: Surface representation of regions on FK1 that experience significant chemical shift changes in the presence of FK506.....	22

Figure 14: $^1\text{H}^{15}\text{N}$ HSQC of FK1 in the presence of tau	24
Figure 15: Intensity ratio plot of ^{15}N -labeled FK1 in the presence of tau.....	25
Figure 16: Surface representation of regions on FK1 That undergo a weak interaction with tau.....	26
Figure 17: Purification workflow for 0N4R tau	28
Figure 18: Post-cleave purification workflow for tau	29
Figure 19: Purification workflow for Hsp90	29
Figure 20: $^1\text{H}^{15}\text{N}$ HSQC for free 0N4R tau	30
Figure 21: Assigned HSQC of 0N4R tau	31
Figure 22: $^1\text{H}^{15}\text{N}$ HSQC for tau in presence of Hsp90.....	32
Figure 23: $^1\text{H}^{15}\text{N}$ HSQC for tau in presence of FKBP51	33
Figure 24: $^1\text{H}^{15}\text{N}$ HSQC for tau in presence of Hsp90 and FKBP51.....	34
Figure 25: Tau associates with Hsp90 and FKBP51 along C-terminal hexapeptide motifs.....	37
Figure 26: Global hairpin orientation of tau allows for further co-chaperone complex association via the N-terminus.....	38
Figure 27. Line shape analysis of most affected residues in hexapeptide regions.....	40
Figure 28. Western blot results of tau and FKBP51 binding to 6X His-tagged Hsp90.	41
Figure 29. Western blot results of ternary complex formation for Hsp90FKBP51 and tau.	42

Figure 30. Structures of the Hsp90, FKBP51 and proposed FKBP51-Hsp90 complex.....	44
Figure 31: Plots of backbone RMSD and distances between geometric centers for the proposed Hsp90-FKBP51 complex model.....	46
Figure 32: Cartoon model of tau's interaction with the Hsp90 – FKBP51 complex.....	53
Figure 33. Protein reference chart.....	57
Figure A1: Dynamic light scattering results	74
Figure A2: Full length intensity ratio plots for tau titrations	100

ABSTRACT

The accumulation of the microtubule associated protein tau has been implicated in several neurological disorders; however, its interaction with chaperones along its normal degradation pathway remains largely uncharacterized at single residue resolution. In this study, nuclear magnetic resonance (NMR) spectroscopy was used to probe the interaction between tau, the molecular chaperone Hsp90, and the immunophilin FKBP51. Resonance intensity changes were observed for specific residues in the heteronuclear single quantum coherence (HSQC) spectra of ^{15}N -labeled tau in the presence of Hsp90 and/or FKBP51. Analysis of the HSQC spectra identified the two hydrophobic hexapeptide motifs located at residues V275 – K280 and V306 – K311 in tau's C-terminal assembly domain as the sites of an interaction with both Hsp90 and FKBP51. Resonances that show reduced intensities did not experience line broadening, which suggests that slow chemical exchange is occurring with a bound conformation that is not observable due to the molecular weight of the complex. We have also investigated the role of the PPIase domain alone in binding to tau and found that specific residues within the PPIase active site experience significant reductions in intensity upon addition of tau. The experimental data is collectively used to propose a structural model for ternary complex formation between tau, Hsp90, and FKBP51.

CHAPTER ONE: INTRODUCTION

Overview of tau biology

The microtubule associated protein tau is localized in the axon tracts of normal neuronal cells and is also an intrinsically disordered protein (IDP) [1-4]. Microtubule associated proteins function as structural proteins of larger cytoskeletal components and are capable of stimulating neuronal growth and development [1,4]. Tau normally functions to bind microtubules (MTs) in the brain and facilitates the stable outgrowth of MT bundles in the axon tracts of developing neurons [1]. Historically speaking, it was not until 1986 that Ihara et al., and Kosik et al. determined that neurofibrillary tangles (NFTs) found in the brain were composed of tau protein [9,10]. In fact, contemporary studies around the same time were the first to reveal that paired helical filaments (PHFs), precursors to NFT formation, contained abnormally high levels of phosphorylated tau protein [11,12].

When tau becomes phosphorylated it will dissociate from MTs, becoming available to enter into its normal degradation pathway. Failure to degrade and recycle higher order tau aggregates leads to the formation of NFTs [13,14]. It is normal for tau to naturally accumulate in our brains as we age, however; toxic NFT formation leads to neurodegenerative defects seen in patients with Parkinson's disease, frontotemporal lobe dementia, Alzheimer's disease (AD),

and other diseases commonly termed “taupathies” [12,15-17]. As many disordered proteins have been shown to be involved in a bevy of human diseases [18], it is not surprising that tau plays such a prominent role in many neurodegenerative disorders.

Protein aggregation is the underlying mechanism behind abnormal tau accumulation because it can effectively halt the maintenance of protein homeostasis [19,20]. Molecular chaperones can function to abrogate protein aggregation by refolding misfolded proteins and promoting the clearance of aggregates through association with other proteins involved in the proteasomal and/or lysosomal degradation pathways [21].

Structure and function of the microtubule associated protein tau

The tau gene is located on chromosome 17q21 and is comprised of one non-coding and 14 coding exons [16,22]. Figure 2 demonstrates that alternative splicing of exons 2, 3, and 10 results in one of six possible tau isoforms that can be grouped into two general categories; those containing three MT-binding repeat domains (isoforms 2N3R, 1N3R, and 0N3R) and those containing four MT-binding repeat domains (2N4R, 1N4R, and 0N4R) [22,23]. Regulating tau expression in this way plays an integral role in the expression of disease phenotypes and will alter the normal function of neurons in the brain.

Although the 0N4R tau isoform is considered entirely disordered, the C-terminal assembly domain, comprised of four MT-binding repeats, is distinctly different than the N-terminal projection domain. The N-terminal domain (residues 1-200) is highly dynamic and has a significantly lower amount of transient

secondary structure when compared to the C-terminal assembly domain (residues 201-441) [24]. Although this can be partially attributed to the high percentage of acidic residues in the N-terminal domain of tau, the presence of repeats in the C-terminal assembly domain creates sequential regions of transient secondary structure near the MT-binding repeats that leads to a decrease in rotational correlation time and a corresponding decrease in dynamics around those regions [24]. The projection domain is not needed for tau to associate with microtubules; however, the presence of variable exons in this domain does play some role in developmental regulation [23-25]. This domain is also where the majority of disease-causing mutations in the tau gene reside, further belying its importance both in tau function and pathogenicity [15,16,26].

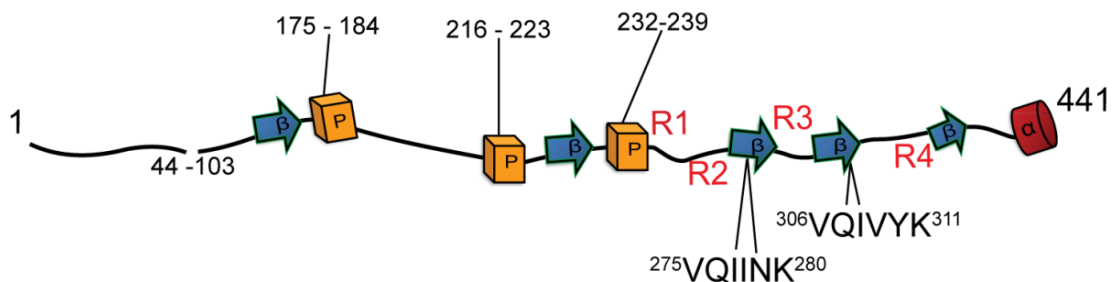


Figure 1. Schematic representation of 0N4R tau. Although tau is intrinsically disordered, it has been shown to form some transient secondary structure in the presence of MTs and other polyanions [33]. Residues 44-103 do not exist in the 0N4R tau construct due to alternative splicing. This schematic highlights hexapeptide V275 – K280 and hexapeptide V306 – K311 in tau’s C-terminal assembly domain and their relative positions preceding MT binding repeats R3 and R4, respectively. These two regions exhibit the highest degree of transient beta sheet structure. The V275-K280 hexapeptide has a fractional content of beta-sheet structure representing 22% of the total population and hexapeptide V306-K311 has a fractional content of beta-sheet structure representing 25% of the total population [31,33].

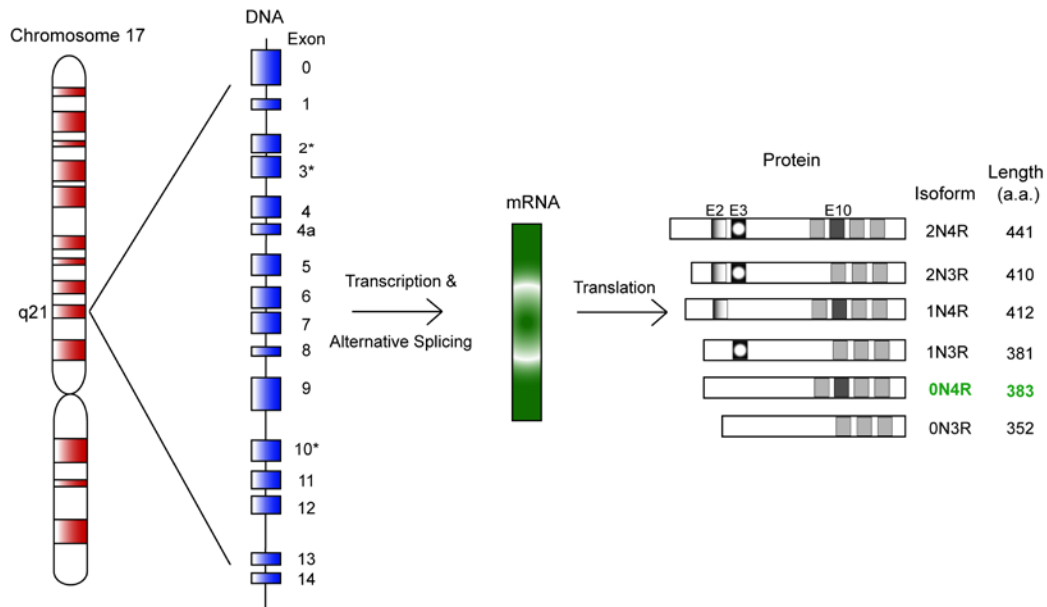


Figure 2. Schematic representation of alternative splicing in the q21 locus of chromosome 17. Alternative splicing on exons 2, 3, and 10 in the q21 region gives rise to different tau isoforms of various lengths. The 0N4R construct used here (highlighted in green) contains all four MT-binding repeat domains and is 383 amino acids long.

Intrinsically disordered proteins in disease

In general, intrinsically disordered proteins are characterized as having a dynamic, extended non-globular structure capable of adopting a broad range of ensembles [27-33]. The lack of tertiary structure and the ability to adopt numerous conformations allows for binding promiscuity with many distinctive protein partners or ligands across various cell types [34,35]. IDPs are common in the proteomes of all species and play prevalent roles in diseases such as cancer and Alzheimer's [18,36]. In terms of evolution, the abundance of IDPs in eukaryotes (predicted to be 15-45% of total proteome) is most likely a result of the increased need for cell signaling and gene regulation in more complex

systems [29,34]. Figure 3 shows a plot of the residue specific disorder tendency.

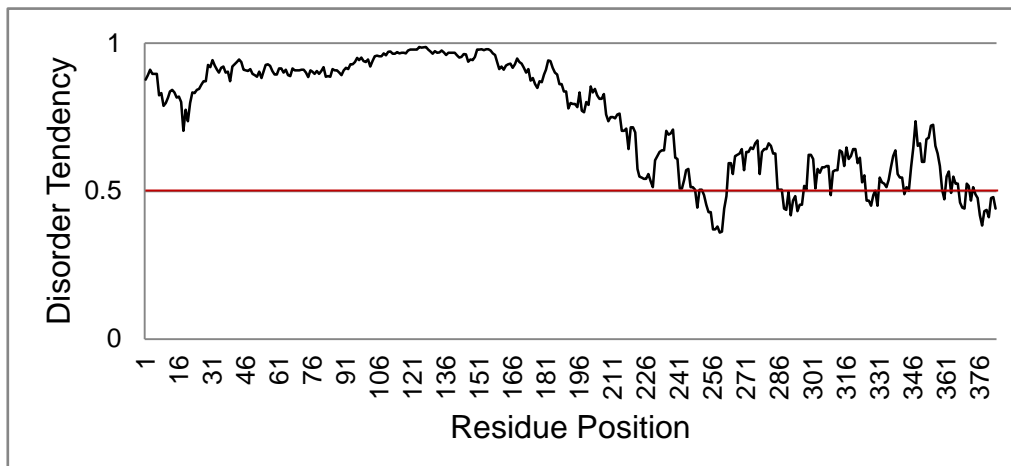


Figure 3. IUPRED Disorder prediction of 0N4R tau. This plot represents the disorder tendency of 0N4R tau. Anything above the redline at 0.5 is predicted to be disordered [5].

When studied experimentally, IDPs have displayed high specificity and low affinity for their respective binding partners and are overrepresented in protein families that are involved in transcription, translation, signal transduction, and cell cycle regulation [28,30,34,37]. Although IDPs have a disordered native state, they can adopt a relatively rigid structure in the presence of a ligand through a process termed coupled folding and binding. This mechanism involves the transition from disorder to order upon association with a binding partner [27,28,30]. When tau associates with itself, the more pronounced transient beta-sheet structure in the assembly domain has been shown to lend itself to the formation of aggregates in the brain. More specifically, tau's normal function of binding and stabilizing MT bundles can be affected by its ability to form transient beta-sheet structure in the C-terminal assembly domain [38].

The function of tau can also be regulated by altering its phosphorylation status resulting in dissociation from MT bundles [25,39]. Tau has over 75 possible phosphorylation sites that are regulated by a host of different kinases and phosphatases [40,41]. In particular, microtubule associated protein kinases and cyclin dependent kinases have been shown to phosphorylate serine and threonine residues along the MT-binding domains of tau [25,42-44]. NFTs containing tau protein have been shown to contain a high amount of the phosphorylated tau species, relative to unphosphorylated tau [25,45]. It is phosphorylated tau that is thought to interact with co-chaperones along its normal processing and degradation pathway *in vivo*. Molecular chaperones that participate in the processing, recycling, and degradation of tau have been implicated in the formation of NFTs [46-51]. Specifically, Hsp90 and its co-chaperone FK506 Binding Protein 51 (FKBP51) have been shown to regulate the status of tau and directly effect levels of both the total and phosphorylated species of tau in the brain [45,50].

The role of molecular chaperones in tau processing

Defining the interaction between tau and proteins along its degradation pathway is important to unraveling the molecular mechanism by which it is processed. Molecular chaperones such as Hsp90 are abundant in brain tissue and are capable of recruiting client proteins to assist along the processing and/or degradation pathway [45,52,53]. Typically, co-chaperone complexes containing Hsp90 can bind a variety of clients with different functions [20,54,55]. FKBP51 assists in recruiting client proteins like tau to the co-chaperone complex and can

even alter the ATPase activity of Hsp90 [19,20]. Although tau is abundant in the brain and naturally accumulates as we age, its physiological concentration relative to Hsp90 and FKBP51 is not known [56]. In recent years, Hsp90 and FKBP51's role in the brain have been studied for their relevance to neurodegenerative disorders such as AD. In 2010, Dickey et al. showed through co-immunoprecipitation studies that FKBP51 co-localizes with Hsp90 and tau in the axon tracts of developing neuronal cells, suggesting evidence for the physical interaction of these proteins *in vivo*. The same study also found that siRNA knockdowns of FKBP51 reduced tau levels, while FKBP51 overexpression enhanced the association of tau with Hsp90 – promoting clearance of aggregates and the outgrowth of microtubules [45]. A surface image of the Hsp90 dimer is presented in Figure 4 and was prepared using Pymol [57].

FKBP51 is an immunophilin and has PPIase activity

The immunophilin family of proteins are typically categorized into the FK506 binding proteins and those that bind cyclosporin A, with both of these sub families showing peptidylprolyl *cis/trans* isomerase (PPIase) activity [58-60]. PPIases get their name because they catalyze a reaction that accelerates the folding of proteins for which the rate determining step involves the isomerization from the *trans* to *cis* conformation of proline peptide bonds [61,62]. The PPIase activity of FKBP51 rests within the FK1 domain with a requirement for residues F67 and D68. Part of this study will focus on providing novel nuclear magnetic resonance (NMR) spectroscopy data regarding the PPIase domain (FK1) of FKBP51 as well as how this domain may interact directly with tau.

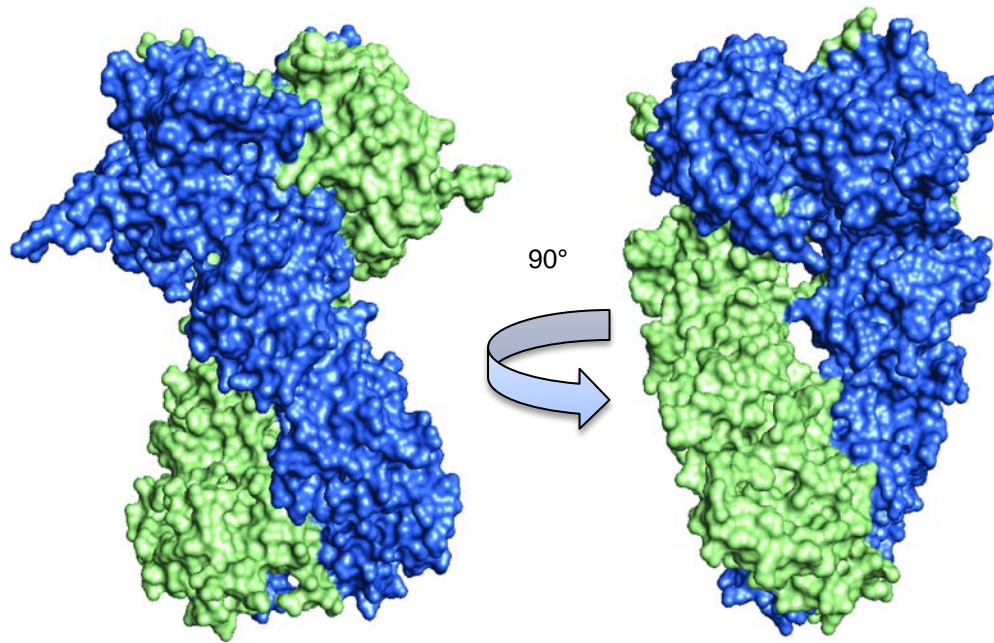


Figure 4. Crystal structure of Hsp90 dimer. Cartoon surface representation of the Hsp90 dimer (derived from PDB ID: 2CG9). Different colors indicate respective Hsp90 monomers in the larger dimer. Co-chaperone complexes containing Hsp90 can bind a variety of client proteins [8].

Previous evidence has shown that a similar PPlase, Pin1, is able to interact with tau and modulate phosphorylation through an interaction with protein phosphatase A [63,64]. It is proposed that Pin1 may interact with tau and catalyze an isomeric change to the *trans* conformation – thereby facilitating a phosphorylation event, although the specific mechanism remains ambiguous [63]. Pin1's ability to regulate dephosphorylation with the assistance of protein phosphatase 2A combined with its inherent PPlase activity is similar to that of FK1; except that Pin1 lacks the Hsp90-interacting tetratricopeptide repeat (TPR) domain present in the full length protein, FKBP51 [6]. The domain structure of FKBP51 is highlighted in Figures 5. It is believed that Hsp90 and FKBP51 form a co-chaperone complex that regulates the recycling of tau. It is thought that the

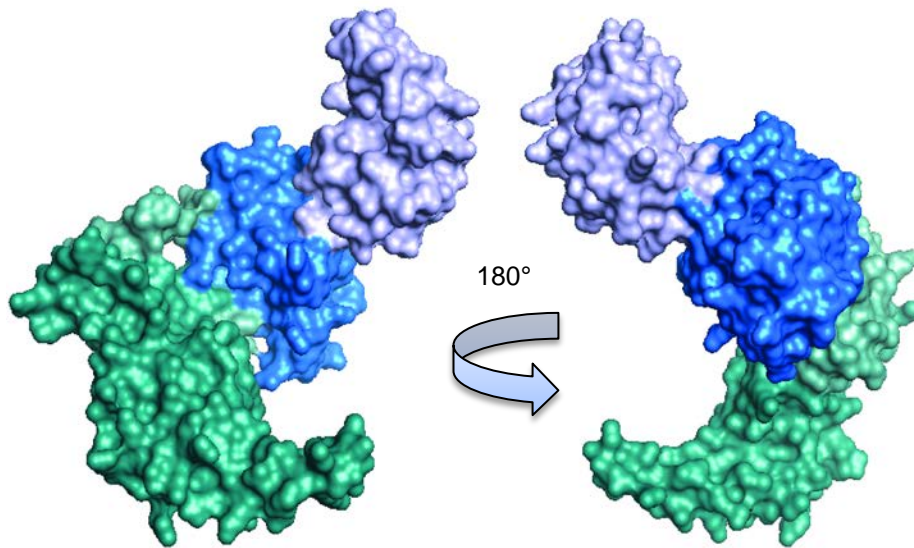


Figure 5. Domain structure of two FKBP51 monomers. Cartoon surface representation of FKBP51 (derived from PDB ID: 1KT0). Colors indicate the three domains of full length FKBP51 – FK1 (purple), FK2 (blue), and the TPR domain (green) [7].

association between FKBP51, Hsp90, and tau collectively functions as a co-chaperone complex and acts as a mechanism for normal degradation and recycling of tau [45,65]. Interestingly, recent cellular studies by Dickey et al. in 2010 have shown that an siRNA knockdown of FKBP51 leads to a reduction of tau levels in neuronal tissue – indicating better clearance of tau aggregates. Conversely, their results show that when FKBP51 is overexpressed in neuronal cells it appears to have a neuroprotective effect; preserving tau and preventing it from degrading normally. Although FKBP51 has been shown to interact with tau via co-immunoprecipitation assays, a physical binding event at single residue resolution has yet to be documented [45]. FKBP51 is also unique among the FKBP5s because it possesses the ability to interact with Hsp90 via a TPR domain, a feature not present in all other FKBP5s [7,66,67]. This interaction is highlighted in

Figure 6. Although a similar FKBP, FKBP52 contains 60% sequence similarity with FKBP51 and includes a TPR domain, cellular studies have demonstrated to have opposite effects on tau regulation - a dichotomous relationship between the function of FKBP51 and FKBP52 [66,67].

Structural considerations of the Hsp90 – FKBP51 co-chaperone complex

Previous studies have shown that the TPR domain on FKBP51 associates with the MEEVD recognition site in the C-terminus of Hsp90. During a study in 2001 looking at the association of known PPlases with Hsp90, Buchner and colleagues determined that Hsp90 and FKBP51 bind tightly, with a K_d of 174nm [67]. In terms of regulating protein homeostasis *in vivo*, the PPlase activity present in the FK1 domain of FKBP51 has been shown to promote tau stability and improve microtubule integrity [6,45,67]. PPlase activity is particularly important in terms of tau biology as cellular studies have shown PPlase deficient mutants of FKBP51 show higher percentages of phospho-tau and total tau aggregates *in vivo* [45]. Understanding how a co-chaperone complex comprised

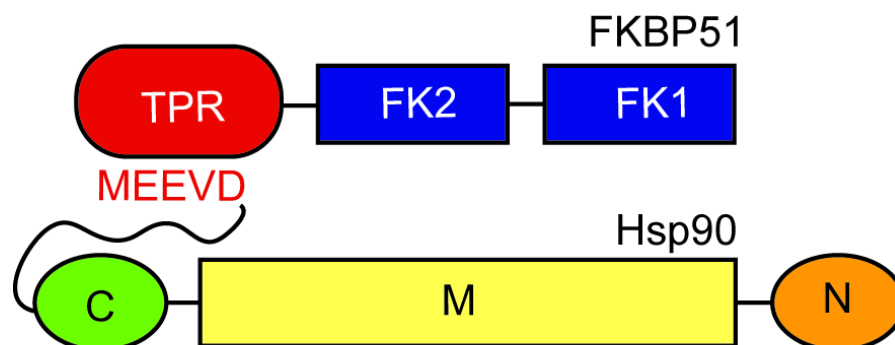


Figure 6. Cartoon model of Hs90 – FKBP51 complex. This cartoon representation of the Hsp90 – FKBP51 co-chaperone complex highlights the interaction between the TPR domain of FKBP51 and the MEEVD sequence on Hsp90.

of one Hsp90 dimer will associate with FKBP51 and interact with tau will facilitate our understanding of how tau aggregation may be regulated by molecular chaperones.

Project Summary and Specific Aims

The microtubule associated protein tau, is localized in the axon tracts of normal neuronal cells. Although tau normally functions to bind and stabilize microtubules, failure to degrade and recycle higher order tau aggregates has been shown to cause neurodegeneration – a feature common in other neurodegenerative diseases termed “taupathies”. Hsp90 and FKBP51 are proteins believed to form a co-chaperone complex with tau [45]. This interaction likely helps regulate the phosphorylation status of tau and promote its stability or degradation [65,68]. Tau is also an intrinsically disordered protein and further characterization of its structure and dynamics could shed light on other diseases involving disordered proteins. If we understand the mechanism by which tau interacts with Hsp90 and FKBP51 during its processing, we can better define how this interaction abrogates tau aggregation in the brain.

The proposed studies focus on the interaction between tau, FKBP51, the PPIase domain of FKBP51, and Hsp90. Recent evidence has been presented suggesting that there is an increase in both total tau and phospho-tau levels *in vivo* when FKBP51 is overexpressed in an AD mouse model [45]. As full length tau is intrinsically disordered and is not a candidate for crystallography, NMR spectroscopy is the best available method to investigate the specific interaction taking place between tau and its co-chaperone complex. Comparison and

characterization of NMR chemical shift data for tau in both free and bound to Hsp90 and/or FKBP51, will allow us to determine the specific regions on tau involved in binding. We propose that by characterizing the structure, dynamics and interactions of tau in the presence of co-chaperones Hsp90 and/or FKBP51, we will be able to better define how a ternary complex is formed. The specific aims are:

Specific Aim 1: Probing the NMR structure and dynamics of tau and FKBP51. Using NMR spectroscopy we will collect chemical shift data on the ¹³C-¹⁵N-labeled FK1 domain of FKBP51. Titration experiments will be designed between FK1 and FK506 and FK1 and tau, and the perturbations of assigned chemical shifts will be monitored.

Specific Aim 2: Investigating formation of a ternary complex between tau, FKBP51, and Hsp90. Using NMR spectroscopy we will collect chemical shift data for ¹⁵N-labeled tau in order to characterize the structural implications of the interaction between tau in the presence of Hsp90 and/or FKBP51. Resin binding assays and MD simulations will also be employed to assess ternary complex formation.

CHAPTER TWO: PROBING THE STRUCTURE AND DYNAMICS OF TAU AND FKBP51

Rationale and Experimental Design

Recent studies have reported the abundance of FKBP51 in normal brain tissue as well in AD brains, resulting in a renewed focus on the determination of its role in neuronal function [45,69-72]. We anticipate that the activity of the PPlase domain in full length FKBP51 affects the normal aggregation of tau and contributes to the formation of higher order aggregates. Our interest in the PPlase domain of FKBP51 stems from evidence suggesting that a PPlase deficient mutant of FKBP51 (F130A) fails to prevent tau from being digested and recycled, leading to a significant increase in total tau levels [45]. This mutant has also been shown to decrease the length of microtubules in neuronal tissue relative to wild type FKBP51 [45].

We are suggesting that there are specific binding regions contained within the PPlase domain of FKBP51 that are capable of interacting with tau. Previous evidence has shown that the PPlase active site/FK506 binding domain is conserved among many FKBP51s, and it is likely that we will see some chemical shifts in this region [62,73]. As mentioned previously, the PPlase domain may also be involved in regulating phosphorylation events, although that is not the focus of this study. In order to assess secondary structure elements present in

FK1, it was necessary to first perform a HNCACB NMR experiment on the free FK1 domain. This allowed us to make resonance assignments for each non-proline residue on the protein. Once resonances assignments are made, a peak list is generated that contains a list of chemical shifts for the amide proton, amide nitrogen, alpha carbon, and beta carbon for each residue. These chemical shifts are available in Table 1 located in Appendix A.

Sample Preparation of ^{15}N -labeled FK1:

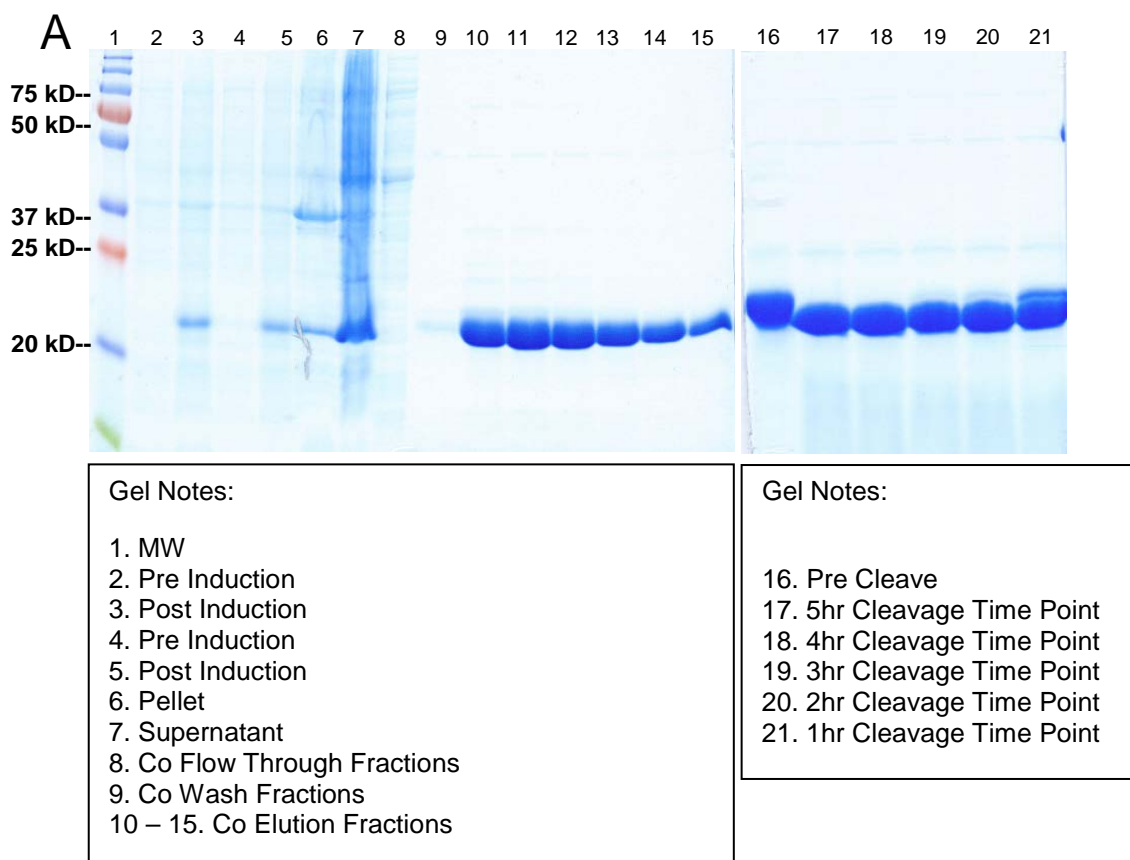


Figure 7A. Purification workflow for FK1. (A) Two gel image for initial affinity Cobalt column (eluted at 3.0 mL/min), and post-cleavage affinity Cobalt column (eluted at 3.0 mL/min), respectively.

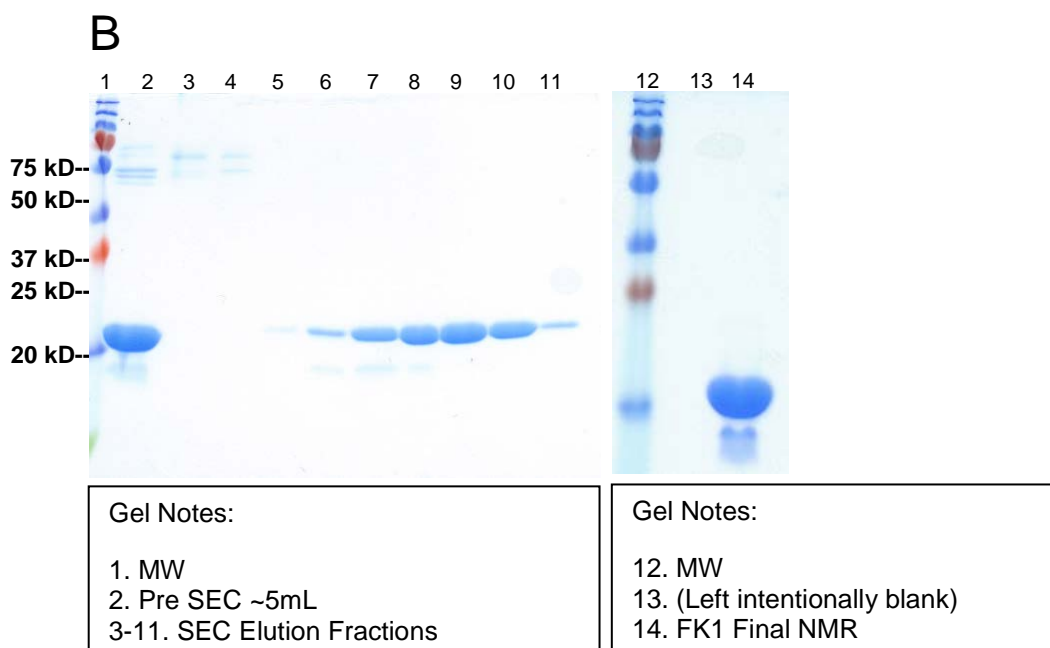


Figure 7B. Post-cleave purification workflow for FK1. (A) Post SEC (eluted at 1.0 mL/min) and gel of final concentrated FK1 NMR sample at 0.483m, respectively.

3D NMR experiments with $^{13}\text{C}^{15}\text{N}$ -labeled FK1

Following the optimization of the purification protocol for FK1, a $^{13}\text{C}^{15}\text{N}$ -labeled protein sample was created using stable metabolic incorporation of isotopic labels. Three neighboring spin systems of the HNCACB spectrum for the $^{13}\text{C}^{15}\text{N}$ -labeled FK1 spectra are shown in Figure 8 below. Once assigned, we can determine the presence of secondary structure by comparing our chemical shifts to standard chemical shift values [74]. All information regarding the NMR data acquisition and processing can be found in the Methods section.

Making resonance assignments

When making new resonance assignments it is necessary to be familiar with the sequence around the region you are assigning. Correlating C_α and C_β chemical shifts from HNCACB spectra can provide information regarding the

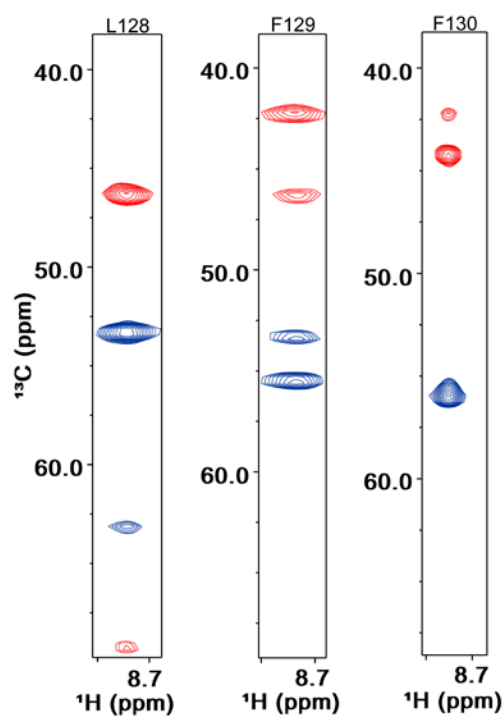


Figure 8. Neighboring spin systems in FK1 HNCACB spectra. This image displays screenshots of neighboring spin systems from spectra used to correlate resonances of L128, F129, and F130 in the FK1 HNCACB spectra. ^1H , ^{13}C , and ^{15}N represent the x, y, and z axes, respectively. Red and blue resonance indicate C_α and C_β , respectively.

backbone structure of the protein of interest. As demonstrated in Figure 8, the positions of the chemical shifts of C_α and C_β in each spin system of the FK1 spectra can be correlated to determine the particular amino acid in and the spin system it corresponds to. The HNCACB requires the protein to have both magnetically labeled N and C atoms and the experiments are designed so that radio frequency pulses induce a resonance effect on the amide proton that is transferred through the covalent bonds to the N, C_α and C_β atoms and back, yielding a signal with resonances in the corresponding frequencies [75]. This allows spectra to be generated in three dimensions with the ^1H , ^{15}N , and ^{13}C

making up the x, z, and y axis respectively. The strongest carbon signal will always come from C_α and C_β atoms of residue i , however; for the HNCACB a weaker resonance coming from the previous residues' C atom, C_β , can also be detected in residue $i-1$. This allows for the correlation of spin systems within the group of spectra generated from the HNCACB, allowing for a more high definition picture of the backbone of the protein.

In the example provided for FK1 in Figure 8, three neighboring spin systems are shown in Figure 8. In the far right spin system for F130, there are stronger resonances for the alpha and beta carbons corresponding to residue F130 (i), and weaker resonances that correspond to the preceding residue, F129 ($i-1$). Spin systems can be connected in this way to eventually correlate each atom for each residue of the protein [75].

Examining secondary structure in FK1

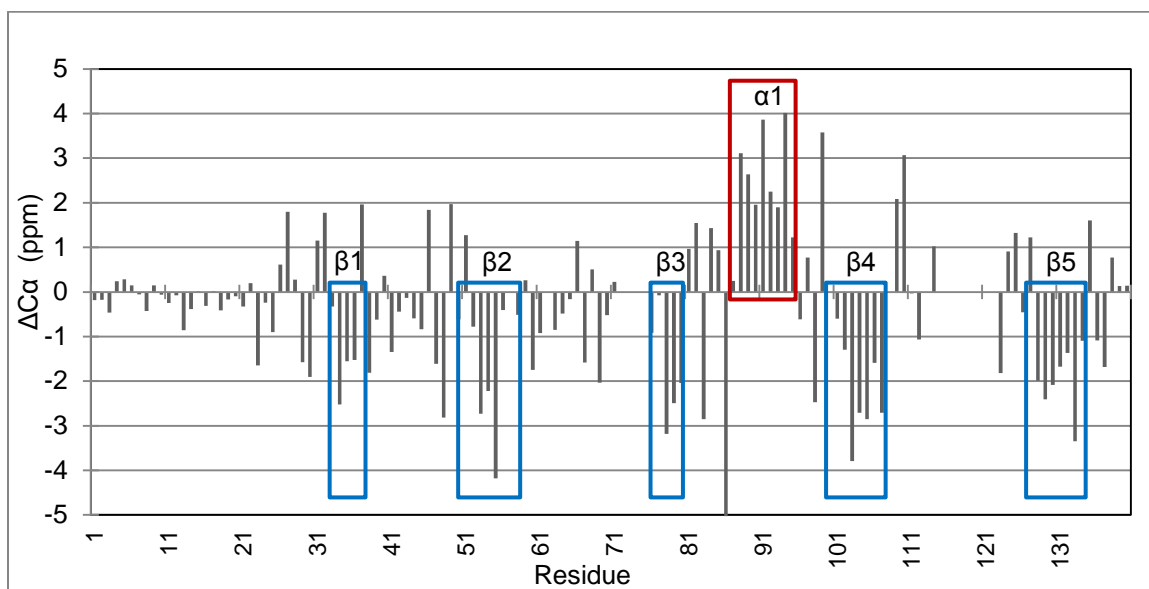


Figure 9. Secondary chemical shift values for the PPlase domain of FKBP51. Values were determined by comparing differences of experimental chemical shifts to standard Peter Wright

random coil values [74]. The Y axis shows the difference between observed and expected chemical shift values. Groupings of three or more residues with chemical shift values greater than or less than 0.7 ppm correspond to predicted α -helix and β -sheet secondary structures, respectively. A full list of chemical shift values for FK1 can be found in Appendix B. Results confirm general structure of five beta sheets surrounding a central alpha helix.

2D NMR experiments with ^{15}N -labeled FK1

In order to further characterize the binding activity of the PPIase domain in the presence of natural product FK506 and also in the presence of tau, an heteronuclear single quantum coherence (HSQC) spectrum was collected for free ^{15}N -labeled FK1 and is shown in Figure 10. This initial HSQC spectrum can easily be used as a benchmark such that once another HSQC spectrum is collected we are able to assess chemical shift and/or intensity changes of resonances undergoing chemical exchange. In order to investigate our hypothesis, we analyzed the different positions and/or intensities of peaks between free FK1 and FK1 bound to FK506. The HSQC for FK1 in the presence of FK506 is shown in Figure 11. The rationale behind performing a titration between FK1 and FK506 prior to FK1 and tau was that because it is a well characterized interaction, the bound state profile of FK1 may shed some light on determining which residues on FK1 are likely to be involved in binding to tau. FK1 was prepared as previously described and tau sample preparation is listed at the beginning of chapter three.

and was titrated into the ^{15}N -labeled FK1 sample. Figure 11 shows an overlay of free ^{15}N -labeled FK1, and ^{15}N -labeled FK1 in the presence of FK506. Figure 12 shows a difference plot of normalized chemical shifts for each assigned residue on FK1 between the free and bound states, respectively. Figure 13 shows an image has also been generated using Pymol that assists in visualizing the correlation between the change in normalized ^1H and ^{15}N chemical shifts (Figure 12) and the location of the conserved binding pocket in the crystal structure of FK1 bound to FK506.

The proton and nitrogen chemical shifts in Figure 12 were combined and normalized using the equation shown in the figure legend. The mean normalized chemical shift was calculated (0.055) for all assigned residues and the red line in Figure 12 indicates one standard deviation above the mean value (0.10). Those chemical shifts that are above the red line indicate resonances experiencing significant chemical shifts, relative to the mean, upon addition of FK506. It is not surprising that these zones are inside and around the binding pocket as shown in Figure 13A and B. Figure 13C show that the backside of the FK1 domain is almost entirely grey, demonstrating that most of the changes, in general, are occurring near the PPlase active site.

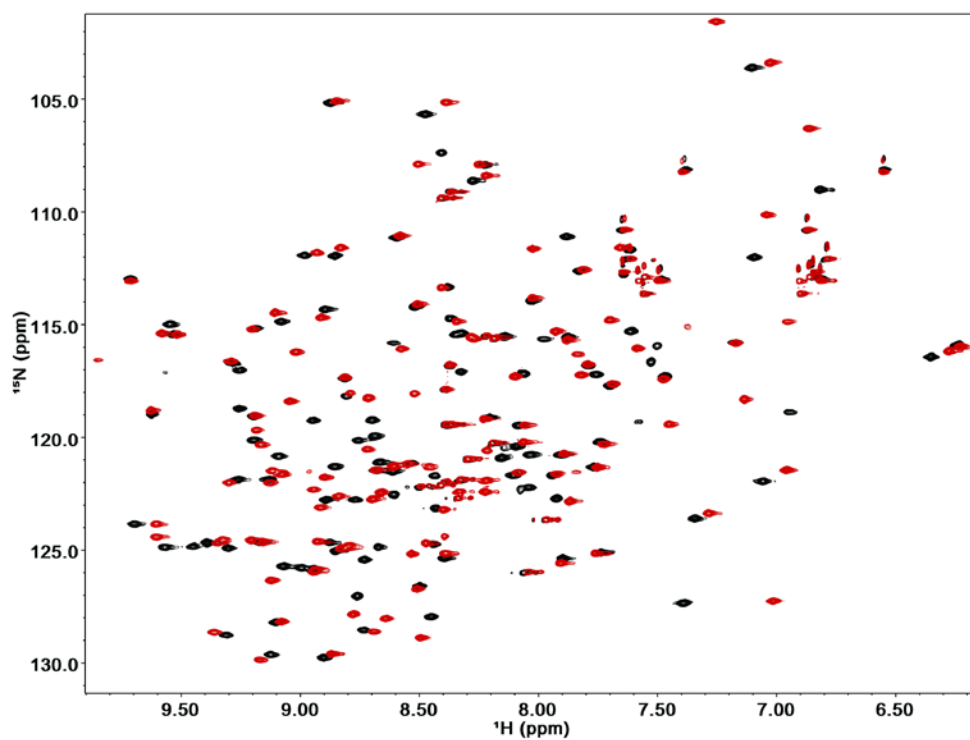


Figure 11. $^1\text{H}^{15}\text{N}$ HSQC ^{15}N -labeled FK1 in the presence of FK506. Overlay of two HSQCs of FK1 in the free state (black resonances) and FK1 bound to FK506 (red resonances).

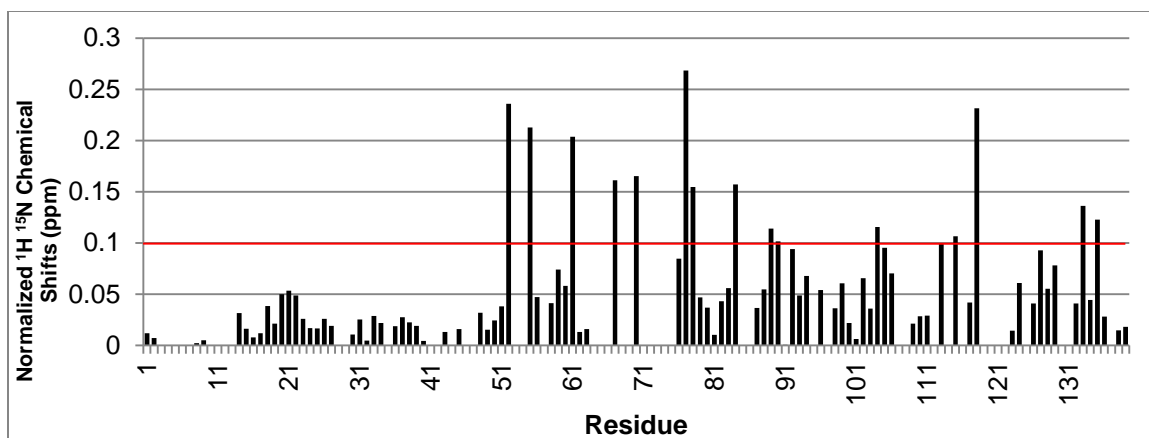


Figure 12. Normalized $^1\text{H}/^{15}\text{N}$ FK1 chemical shift differences between free FK1 and FK1 bound to natural product FK506. ^1H and ^{15}N chemical shift differences for free FK1 and FK1 in the presence of FK506 were normalized together and plotted. One standard deviation above the mean value is indicated by the red line and was calculated from the mean (.056) of the normalized chemical shifts for all residues. Normalization equation: $\sqrt{\frac{(H_1 - H_2)^2 + (N_1 - N_2)^2}{5}}$

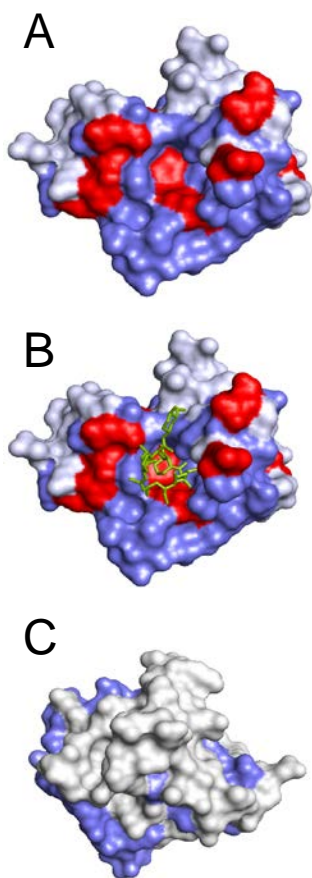


Figure 13. Surface representation of regions on FK1 that experience significant chemical shift changes in the presence of FK506. (A) Displays a surface representation of FK1 bound to FK506, however; FK506 has been removed to show the conserved binding pocket in FK1. Gray indicates regions or residues of normalized ^1H and ^{15}N chemical shift values below the mean. Blue indicates regions or residues with normalized chemical shifts between the mean value and one standard deviation above the mean (0.106) and red indicates normalized chemical shifts that are greater than one standard deviation above the mean. (B) Displays a surface representation of FK1 bound to FK506 with FK506 included (green) [6]. (C) Shows the backside (180° rotation) of FK1 and indicates a lack of intensity changes.

Characterization of FK1 binding to tau

Following spectral analysis between FK1 in the free state and in the presence of tau, we determined that there are no significant global chemical shift changes observed in the spectra. This overlay is shown in Figure 14A. However, there are several important residues that experience changes in intensity and/or experience a small chemical shift. The largest chemical shift occurs for residue I87, which is shown in Figure 14B. Analysis of resonance intensities revealed an important pattern. Figure 15 shows an intensity ratio plot for free FK1 and FK1 in the presence of tau. The plot demonstrates that there are not very many regions that are undergoing significant intensity reductions, however; there are specific residues that are undergoing significant changes. In a normal binding interaction there are typically shorter regions of amino acids (3-6 residues) that are involved in binding. In this case, the only residues that collectively experience an intensity reduction at or greater than one standard deviation above the mean occur in one or two residue gaps. Interestingly, these residues are within regions shown to have strong beta sheet structure determined by our HNCACB experiments (Figure 9) and are also important when FK1 binds to its natural product FK506. The aspartic acid at position 68 experiences the largest reduction in intensity upon addition of tau and is directly linked to PPlase rotamase activity [6,62].

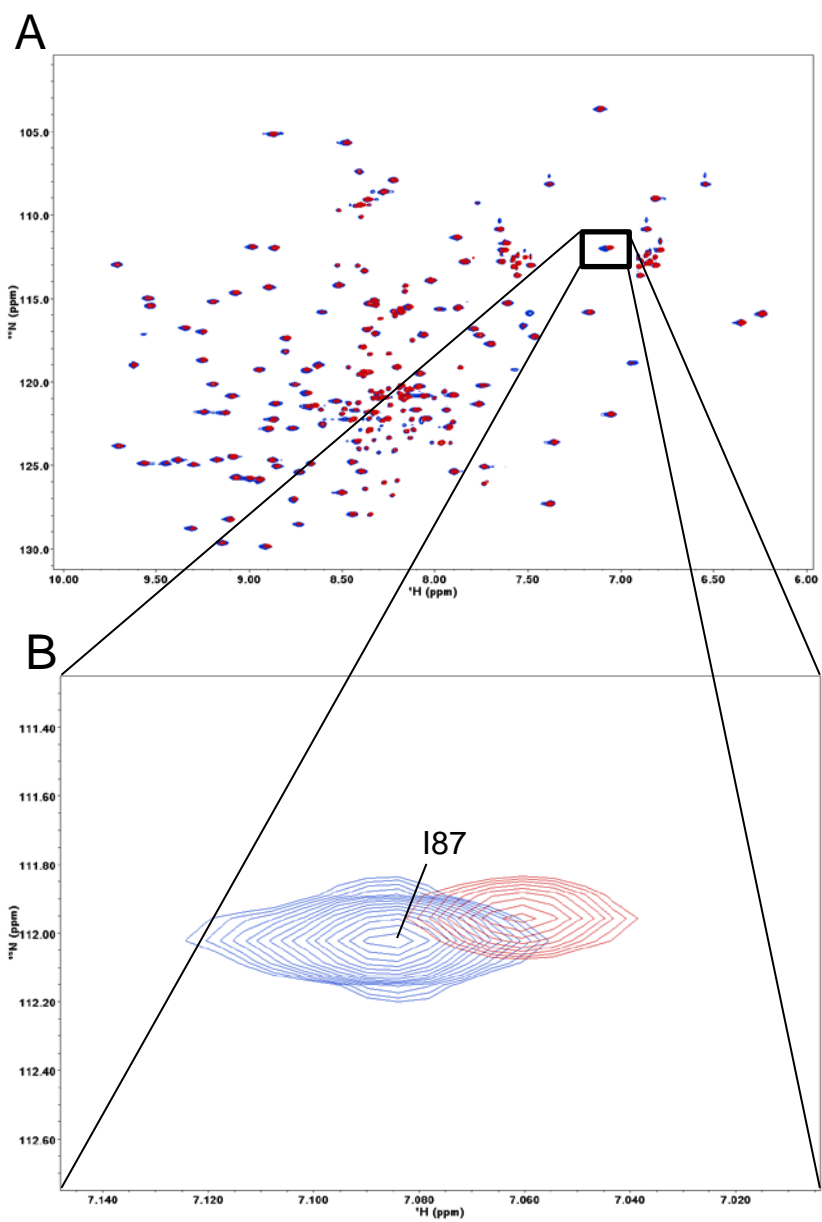


Figure 14. $^1\text{H}^{15}\text{N}$ HSQC of FK1 in the presence of tau. (A) Overlay of two 2D HSQC of FK1 in the free state (blue resonances) and FK1 in the presence of 0N4R tau (red resonances). (B) Residue I87 is in the PPIase active site and experiences the largest chemical shift.

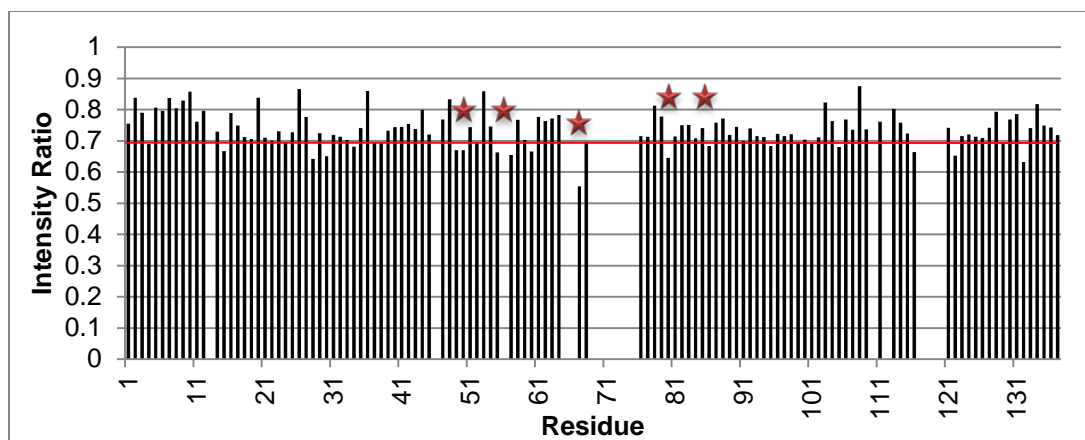


Figure 15. Intensity ratio plot of ^{15}N -labeled FK1 in the presence of tau. The residue that experiences the largest reduction in intensity upon addition of tau is D68. Specifically, H56 and K58, K60 and L61, and D68, F77, S69 and I87, all show reductions more than are one standard deviation outside of the mean. The red line on indicates one standard deviation below the mean and was calculated from the average intensity ratios for all assigned residues. Gaps indicate unassigned or missing resonances. Red stars correspond the red region in Figure16 that experiences the largest changes upon addition of tau.

Analysis of resonance intensity ratio plot for ^{15}N -labeled FK1

Despite the lack of large regional changes seen in the intensity ratio plot in Figure 15, the results show that several residues within the PPLase active site (50-130) do individually undergo significant reductions. Specifically, H56 and K58, K60 and L61, and D68, F77, S69 and I87, all show reductions more than one standard deviation outside of the mean. As these residues are within the region that forms a cleft near residue 68, it is logical that a weak interaction with tau may be taking place in this ready-made pocket. In fact, the initial crystal structure of FK1 bound to FK506 identified several of these residues as important in binding to FK506 [6]. Although D68 has been shown to specifically confer

PPlase activity, the surrounding residues play an important role in positioning the ligand into the binding site. The results presented here demonstrate that previously identified residues important for binding FK506 may also be important for binding to tau, as see in Figure 16 below. The presence of the FK2 and TPR domain may need to be present in order to facilitate a stronger association between the FK1 domain and tau. Although it is beyond the scope of this project, phosphorylated tau species may very well interact differently with FK1 than unphosphorylated tau.

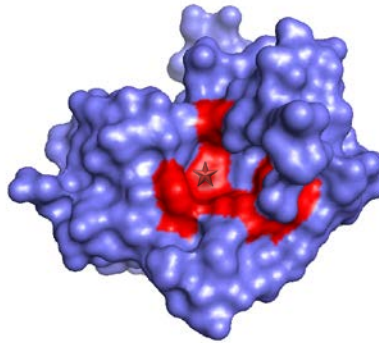


Figure 16. Surface representation of regions on FK1 that undergo a weak interaction with tau. Regions colored red indicate residues that experiencing the most significant intensity reductions. Red stars from Figure 15 correspond the PPlase active site seen in red here [6].

CHAPTER THREE: ASSESSING FORMATION OF A TERNARY COMPLEX BETWEEN TAU, HSP90, AND FKBP51 USING NUCLEAR MAGNETIC RESONANCE SPECTROSCOPY

Rationale and Experimental Design

Tau is an intrinsically disordered protein that binds tubulin in order to facilitate the stabilization and outgrowth of microtubule bundles in the axon tracts of normal neuronal cells [1-4]. Although tau's specific mechanism of processing and degradation in the brain remains ambiguous, it is clear that improper processing of tau by molecular chaperones can lead to the accumulation of aggregates resulting in the formation of neurofibrillary tangles. These tangles are one of the factors implicated in over 15 neurodegenerative disorders, including Parkinson's disease, frontotemporal dementia, and Alzheimer's disease (AD) [12,15-17]. Molecular chaperones that participate in the processing, recycling, and degradation of tau have been implicated in the formation of neurofibrillary tangles [51,79-83]. In particular, the molecular chaperone Hsp90 and its co-chaperone FKBP51 have been shown to regulate the status of tau in the brain but the structural basis for this interaction remains unresolved [45,50,68].

NMR spectroscopy was used to investigate the interaction between tau, Hsp90, and FKBP51. Binding experiments were performed with ¹⁵N-labeled 0N4R tau in the presence and absence of unlabeled Hsp90 and/or FKBP51. For titrations between tau and Hsp90 or tau and FKBP51, two samples of tau at the

same concentration were mixed with a stoichiometric excess (approximately 2:1 see Figure 27B for SDS-PAGE gel image) of either Hsp90 or FKBP51. After HSQC spectra were collected, these two samples were combined and re-concentrated to create a sample containing all three proteins as shown in the last lane of Figure 27B. An HSQC spectrum was then collected for tau in the presence of both Hsp90 and FKBP51. All three HSQC spectra were compared to the initial spectrum of free tau to look for chemical shifts or resonance intensity changes. Figures 22, 23 and 24 all show similar resonance intensity reduction profiles in the presence of Hsp90 and/or FKBP51. Specifically, residues that were mostly localized to the C-terminal assembly domain of tau experienced the largest resonance intensity reductions upon addition of Hsp90 and/or FKBP51.

Sample Preparation of 0N4R tau

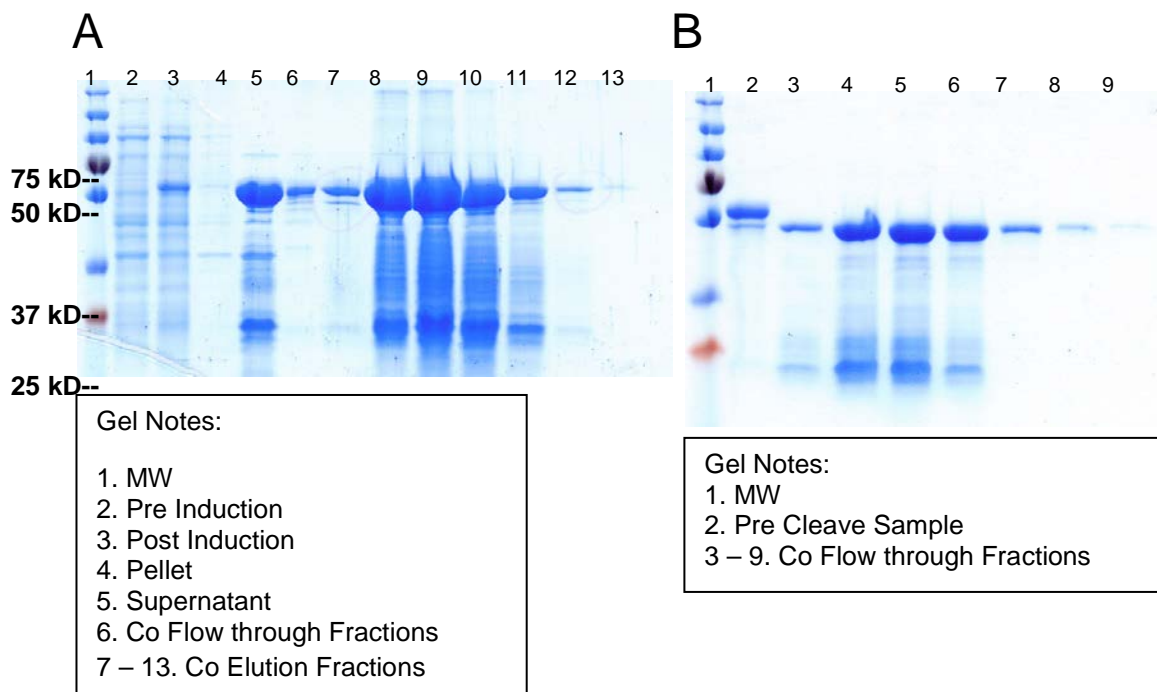


Figure 17. Purification workflow for tau. (A) Gel image for initial affinity Cobalt column (eluted at 3.0 mL/min) and (B) Post-cleavage affinity Cobalt column (eluted at 3.0 mL/min).

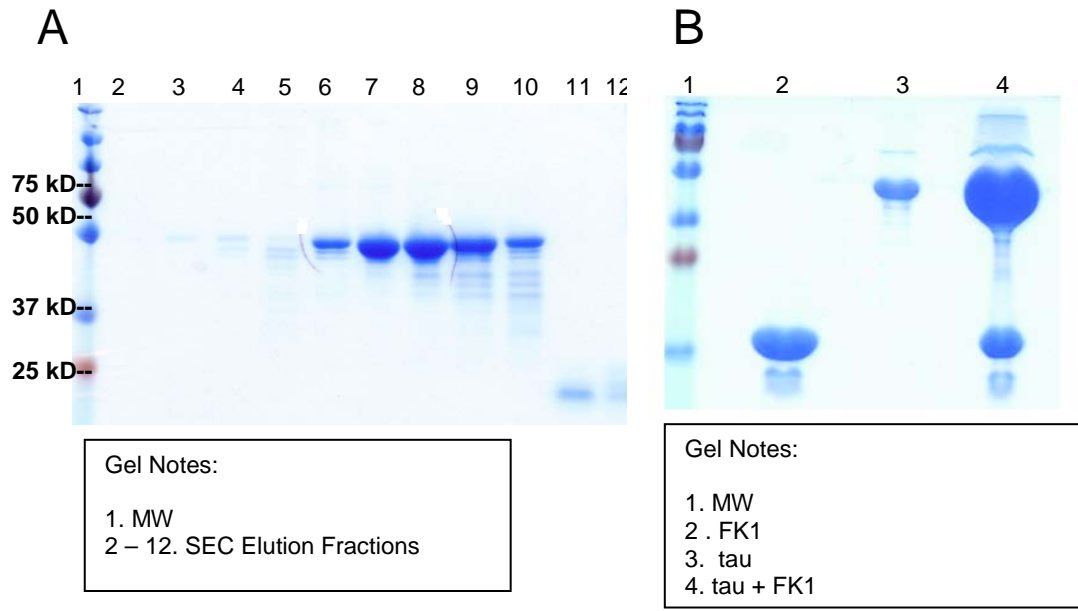


Figure 18. Post-cleave purification workflow for tau. (A) Post SEC (eluted at 0.5 mL/min) (B) Final Gel Image of FK1 (lane 2), tau (lane 3), and FK1 in the presence of tau (lane 4).

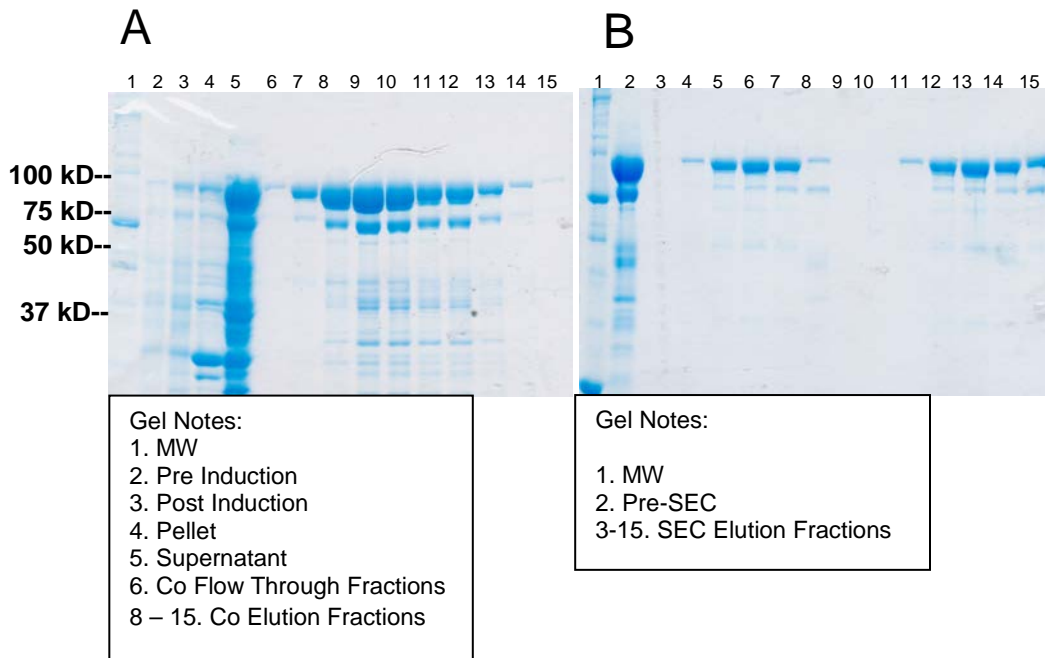


Figure 19. Purification workflow for Hsp90. (A) Gel image for initial affinity Cobalt column (eluted at 3.0 mL/min). (B) (A) Post SEC (eluted at 0.35 mL/min).

2D NMR experiments with ^{15}N -labeled 0N4R tau

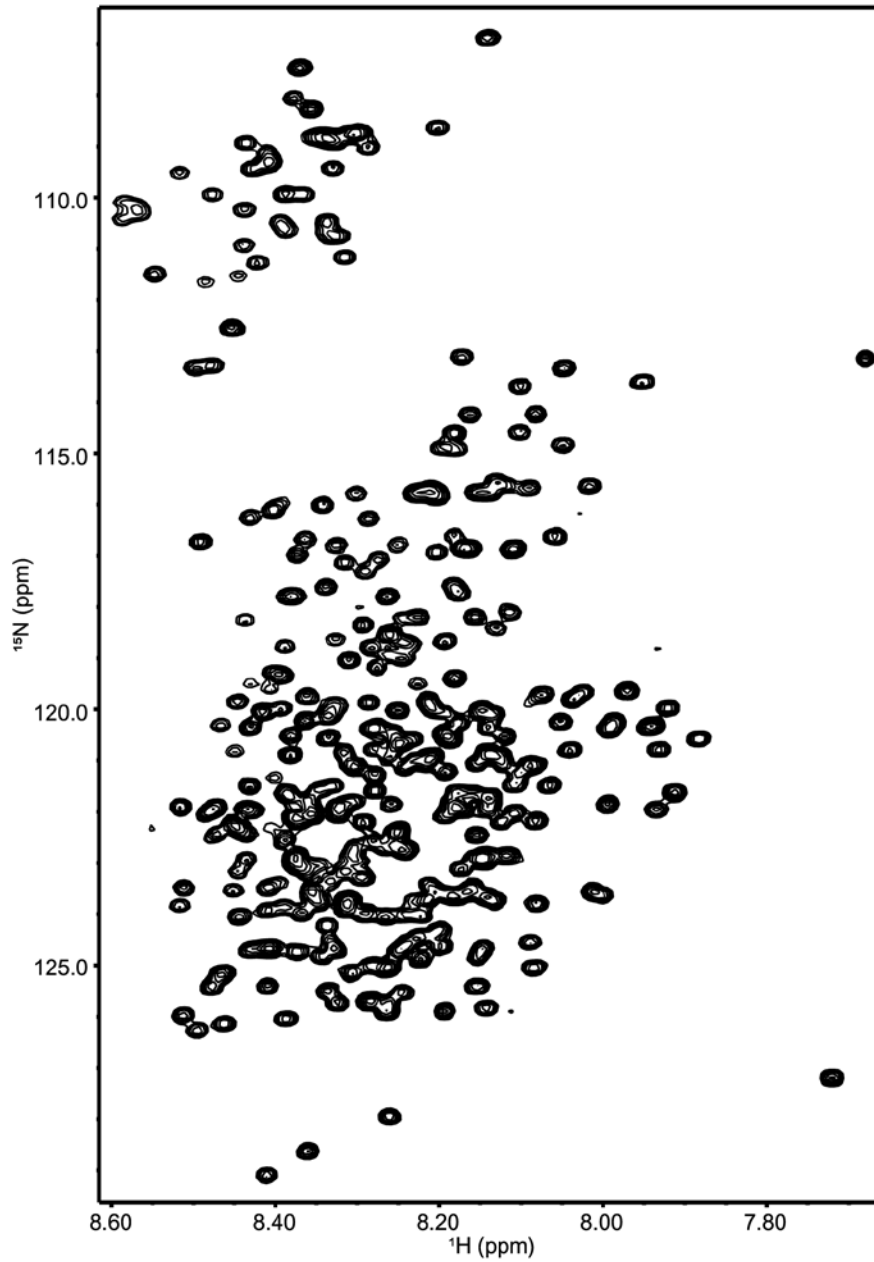


Figure 20. ^1H ^{15}N HSQC for free 0N4R tau. This HSQC of 0N4R tau in the free state at a concentration of 0.1 mM will be used as a benchmark to measure any chemical shifts or intensity reductions for resonances upon addition of a potential binding partner.

the low amount of signal dispersion seen in the hydrogen dimension of the spectra.

After collecting a spectrum for free tau and making resonance assignments another protein can be added to the sample and another HSQC can be collected to look for changes in chemical shifts or intensity reductions.

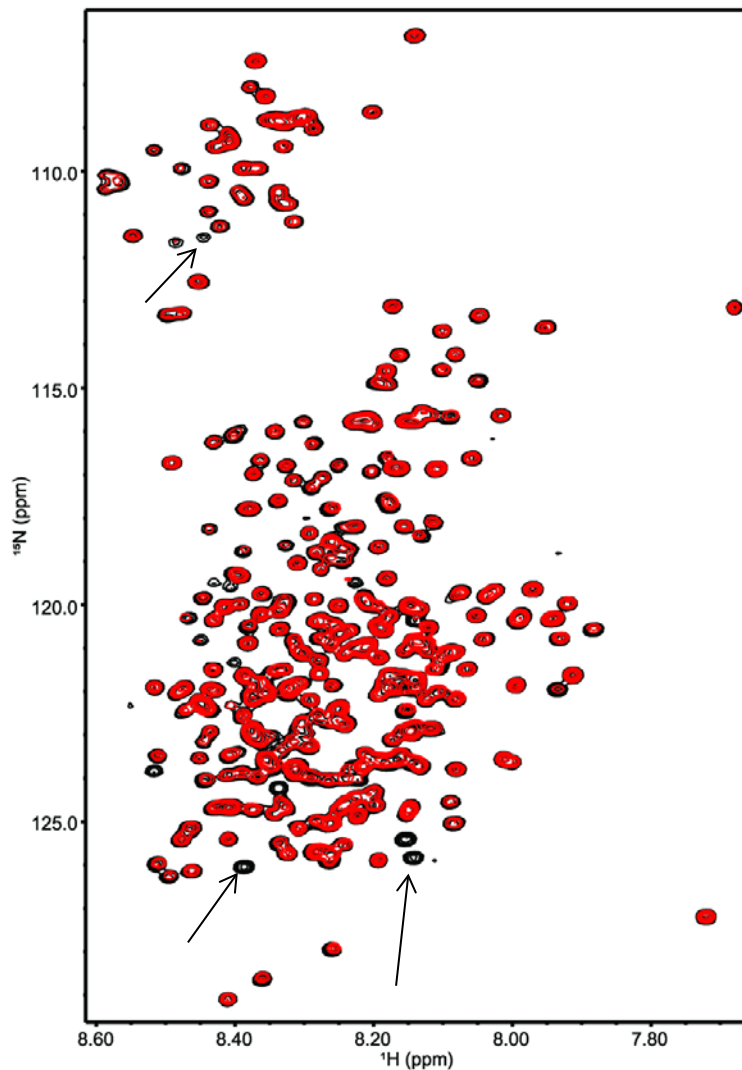


Figure 22. $^1\text{H}^{15}\text{N}$ HSQC for tau in presence of Hsp90. This is an overlay of the free tau HSQC spectrum (black resonances) from Figure 20 and a new HSQC spectrum (red resonances) taken of tau in the presence of Hsp90. Arrows indicate resonances in the C-terminal assembly domain on tau that become significantly less intense in the presence of Hsp90.

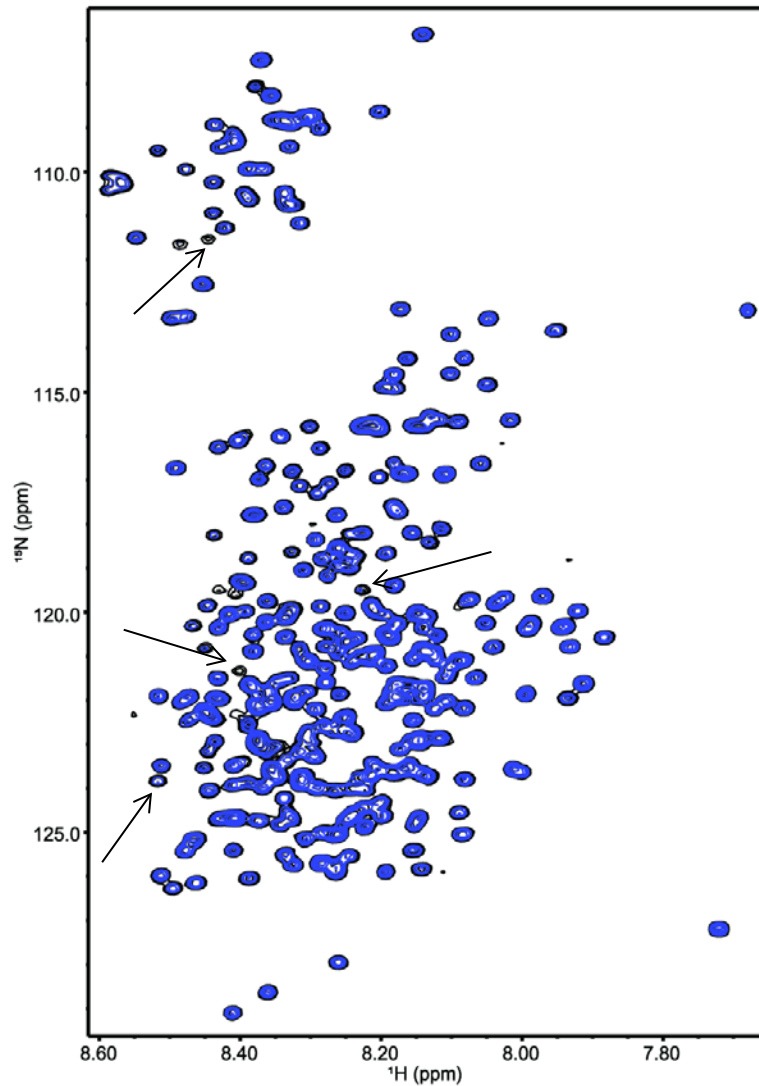


Figure 23. $^1\text{H}^{15}\text{N}$ HSQC for tau in presence of FKBP51. This is an overlay of the free tau HSQC spectrum (black resonances) from Figure 20 and a new HSQC spectrum (blue resonances) taken of tau in the presence of FKBP51. Although the effect of FKBP51 is not as great as that of Hsp90 in tau binding, there is a similar intensity reduction profile in the hexapeptide regions of tau.

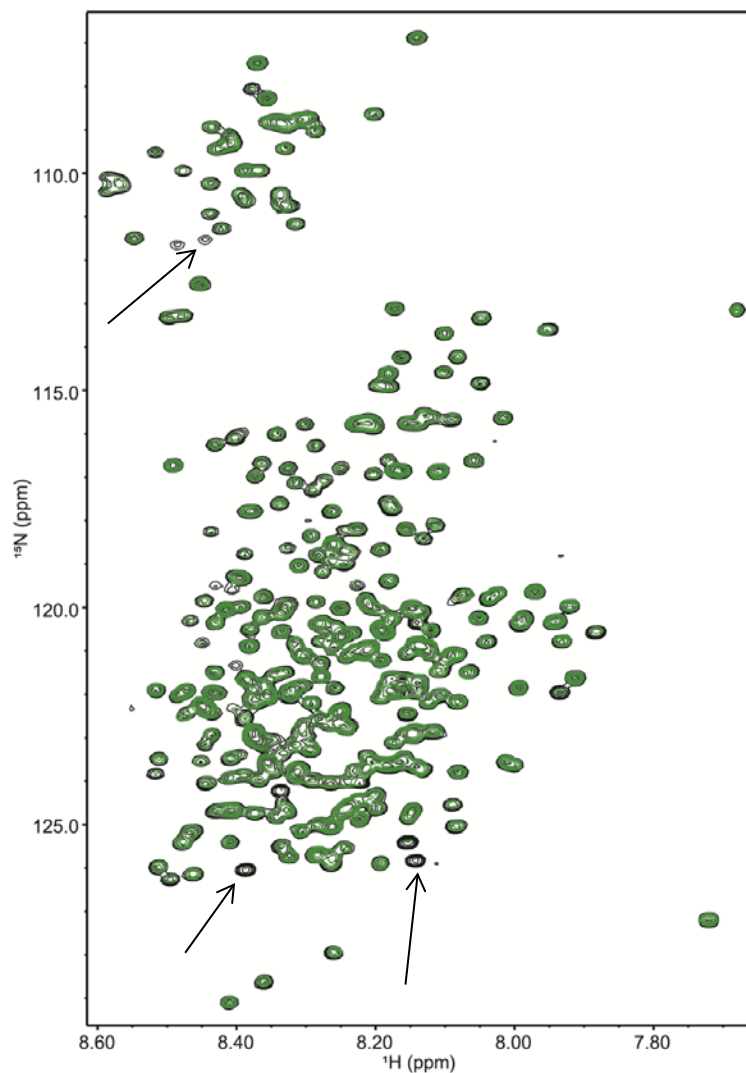


Figure 24. $^1\text{H}^{15}\text{N}$ HSQC for tau in presence of Hsp90 and FKBP51. This is an overlay of the free tau HSQC spectrum (black resonances) from Figure 20 and a new HSQC spectrum (green resonances) taken of tau in the presence of Hsp90 and FKBP51.

Analysis of resonance intensity ratios

To identify individual residues from tau that are important for binding to FKBP51 and/or Hsp90, residue specific resonance intensities were measured for free tau and tau in the presence of Hsp90 and/or FKBP51 [77]. Due to the large molecular weight of the complex no chemical shifts are observable by NMR.

However, intensity ratios between the free and bound spectra can be directly measured and compared to determine which residues are experiencing significant changes in the presence a ligand. These intensity ratios are plotted for residues 270-441 in Figure 25 and for residues 10-40 in Figure 26. Intensity ratio plots for all assigned residues on tau can be found in Appendix D. Each plot is color coded such that red bars indicate intensity ratios between free tau and tau in the presence of Hsp90, blue bars indicate intensity ratios between free tau and tau in the presence of FKBP51, and green bars indicate intensity ratios between free tau and tau in the presence of both Hsp90 and FKBP51. The intensity ratios for tau in the presence of both Hsp90 and FKBP51 were divided by two to account for the doubling of tau concentration when the individual samples of tau plus Hsp90 and tau plus FKBP51 were mixed and re-concentrated. The pink line on each plot indicates one standard deviation below the mean and was calculated from the average intensity ratios for all assigned residues.

Intensity ratios that are more than one standard deviation below the average value are probably involved in complex formation. As seen in Figure 25, intensity ratios in this category are observed for residues V275 – K280 and V306 – K311. These residues form the hydrophobic hexapeptide motifs mentioned above, and precede MT-binding repeat domains R2 and R3. These regions were previously identified as being important for binding to Hsp90 and are necessary for the formation of paired helical filaments that lead to the formation of neurotoxic aggregates [38,85,86].

Figures 25A and 25B demonstrate tau's ability to bind independently to Hsp90 and FKBP51 and indicate the presence of overlapping binding sites in the hexapeptide regions of tau. Figure 25C shows what happens when all three proteins are mixed together, which should result in ternary complex formation. The intensity reductions observed in Figure 25C are not additive with respect to Figures 25A and 25B and it appears that the binding of Hsp90 dominates the effect seen in both hexapeptide motifs. This suggests that ternary complex formation is non-cooperative and the interaction between Hsp90 and tau is stronger than the interaction between FKBP51 and tau. It is important to note that the tau samples used in this study are unphosphorylated, while the form of tau that interacts *in vivo* with Hsp90 and FKBP51 is thought to be hyperphosphorylated [45].

N-terminal residues in tau are involved in association with the co-chaperone complex

Intensity ratio plots in Figure 26 show that upon addition of Hsp90 and/or FKBP51, several residues near the N-terminus of tau also experience significant intensity reductions. However, intensity reductions in this region are not as large as those observed for the two hexapeptide motifs. Interestingly, the magnitude of the residue specific intensity reductions is greater for FKBP51. This can be seen by comparing Figures 26A and 26B. In Figure 26A, only one of the residues (E9) has an intensity ratio that is more than one standard deviation below the average. In contrast, a significant reduction is seen for the resonance intensities for residues 9, 10, 12-14, and 16 upon addition of FKBP51, as shown in Figure

26B. In Figure 26C, it appears this effect is amplified in the presence of both proteins. This suggests that the residues in the N-terminus of tau play some role in the formation of the Hsp90-FKBP51 complex either via self-interaction with the C-terminus or by making further contacts with the co-chaperone complex. This complements previous NMR and FRET data demonstrating tau's ability to form a double hairpin or paperclip structure in which the N-terminus is transiently localized near the C-terminal assembly domain [24,87].

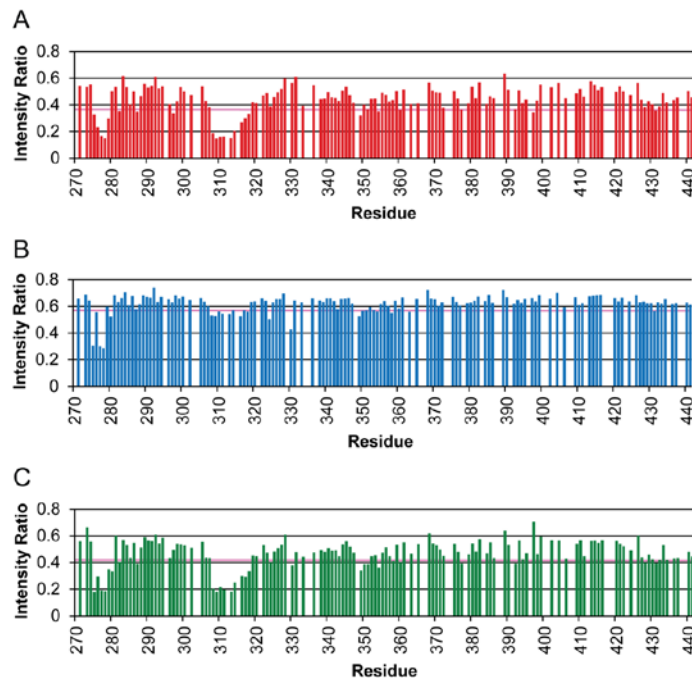


Figure 25. Tau associates with Hsp90 and FKBP51 along C-terminal hexapeptide motifs. (A) Intensity ratio plots for ^{15}N -labeled tau in the presence of Hsp90. The two regions that experience the largest reductions are two hydrophobic hexapeptide regions, V275 – K280 and V306 – K311. (B) Intensity ratio plots for tau in the presence of FKBP51 show that tau has overlapping binding sites for Hsp90 and FKBP51. (C) The intensity ratios for ternary complex formation between tau and its molecular chaperone complex are additive when compared to tau bound to FKBP51 alone. Intensity ratios were determined by dividing the intensity of each resonance in the presence of Hsp90 and/or FKBP51 by the intensity of free tau. The pink line on each plot indicates one standard deviation below the mean and was calculated from the average intensity ratios for all assigned residues.

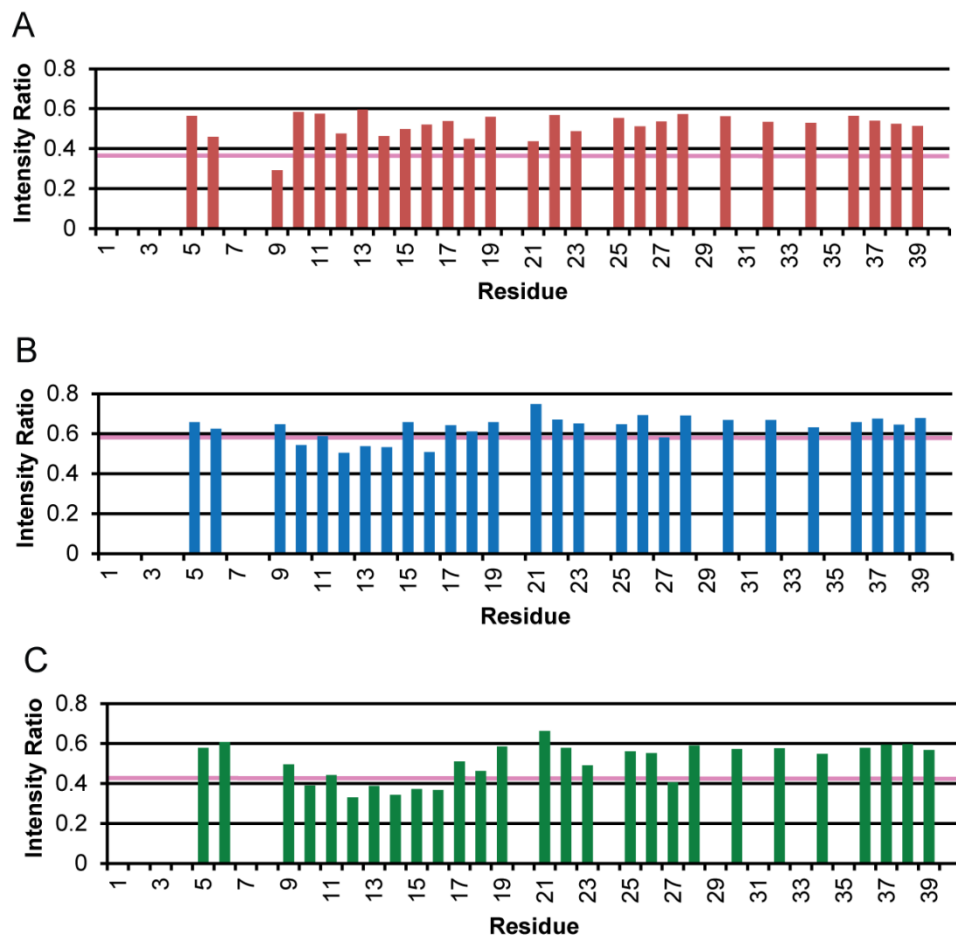


Figure 26. Global hairpin orientation of tau allows for further co-chaperone complex association via the N-terminus. (A) Intensity ratio plots for tau residues 1 – 40 show minimal intensity ratio reductions upon addition of Hsp90 to free tau. (B) Tau shows a stronger interaction in its N-terminus in the presence of FKBP51 as compared with tau in the presence of Hsp90. (C) However, upon conglomeration of all three proteins together, the largest reduction in resonance specific intensity ratios are observed. Intensity ratios were determined by dividing the intensity of each resonance in the presence of Hsp90 and/or FKBP51 by the intensity of free tau.

Line shape analysis of the most affected resonances in the hexapeptide regions

In the presence of both Hsp90 and FKBP51, resonances in the two hexapeptide motifs show reduced signal intensity in the absence of line broadening in the hydrogen dimension. This is shown in Figure 27 for some of the most affected residues in each hexapeptide region, I278 and N279, and V309 and Y310. These figures show an overlay of projections along the hydrogen frequency dimension for all four spectra. Resonances that show reduced intensity in the absence of line broadening are probably undergoing chemical exchange with a bound conformation on a relatively slow timescale. A dissociation constant (K_d) in the low micromolar to nanomolar range can be inferred for residues that experience slow chemical exchange [76,77].

However, the behavior of the resonances shown in Figure 27B is not consistent with the presence of a two-fold excess of either Hsp90 or FKBP51. If the K_d is in the low micromolar range then a two-fold excess of either binding partner should saturate binding and lead to the complete disappearance of the free resonances. Since this did not occur we must assume that all of the Hsp90 and FKBP51 that was titrated with tau was not competent for binding. This hypothesis was partially confirmed by performing dynamic light scattering (DLS) on concentrated samples of Hsp90 and FKBP51, which showed limited but significant evidence for aggregation of both proteins (Appendix A). When smaller systems undergo slow exchange, a resonance for the bound state may be observed. This is not the case for tau binding to either FKBP51 or Hsp90 because the mass of the complex is beyond the range of detection for a standard

HSQC experiment. HSQC-TROSY experiments also failed to resolve bound resonances for the tau-FKBP51 complex or the tau-Hsp90 complex.

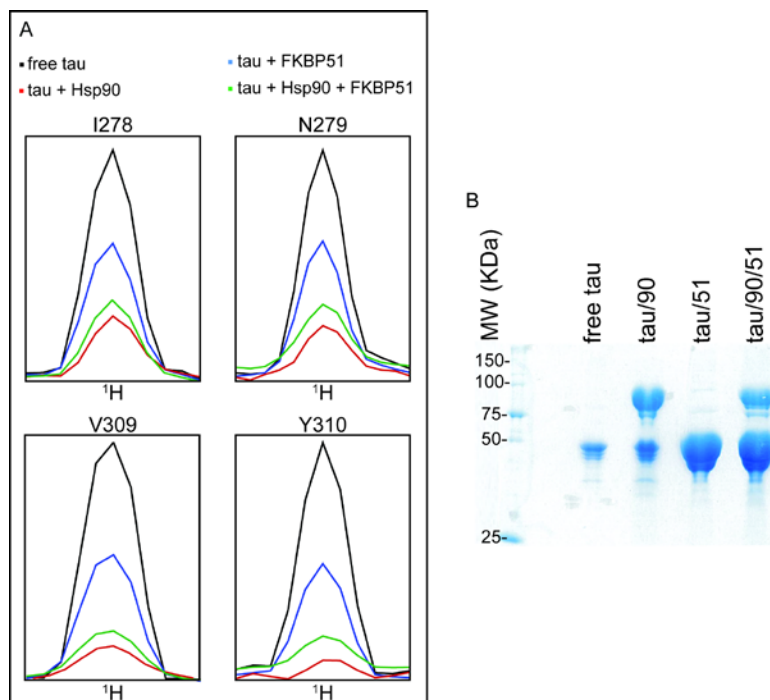


Figure 27. Line shape analysis of most affected residues in hexapeptide regions. (A) Overlay of 1D projections along the hydrogen frequency dimension for all spectra. Line traces show the most affected residues in each of tau's hydrophobic hexapeptide motifs – I278 and N279 from the V275 – K280 hexapeptide, and V309 and Y310 from the V306 – K311 hexapeptide. Free tau is indicated by the black line. Red lines correspond to the tau-Hsp90 complex, blue lines correspond to the tau-FKBP51 complex, and green lines correspond to tau in the in a ternary complex with Hsp90 and FKBP51. These resonances experience reduced intensities in the absence of line broadening in the presence of Hsp90 and FKBP51. (B) 10% SDS-PAGE gel of final purified proteins used for NMR titrations. Gel lanes from left to right: (1) MW Protein Marker (Page Ruler Plus), (2) 0N4R tau, (3) 0N4R tau + Hsp90, (4) 0N4R tau + Hsp90, and (5) 0N4R tau + Hsp90 + FKBP51.

Resin binding assay to confirm ternary complex formation

This section describes a binding assay that was developed based on the property that proteins possessing a 6X His-tag will bind to Cobalt resin. Since Hsp90 is the largest protein and likely forms the core of a co-chaperone complex capable of interacting with tau the 6X His-tag was used to immobilize no more than 5 mg of Hsp90 to 500 μ L of Co resin equilibrated in Co A1 binding buffer (See Methods for specifics buffer recipes). Subsequently, untagged proteins (tau and FKBP51) were applied to the column and incubated with Hsp90. The resin was washed to remove any non-specific bound proteins. Hsp90 was then eluted; presumably with tau and/or FKBP51 bound (a detailed protocol for the cobalt binding assay can be found in the methods section). Fractions collected were run against antibodies for Hsp90, tau and FKBP51. Those results are presented in Figures 28 and 29 below.

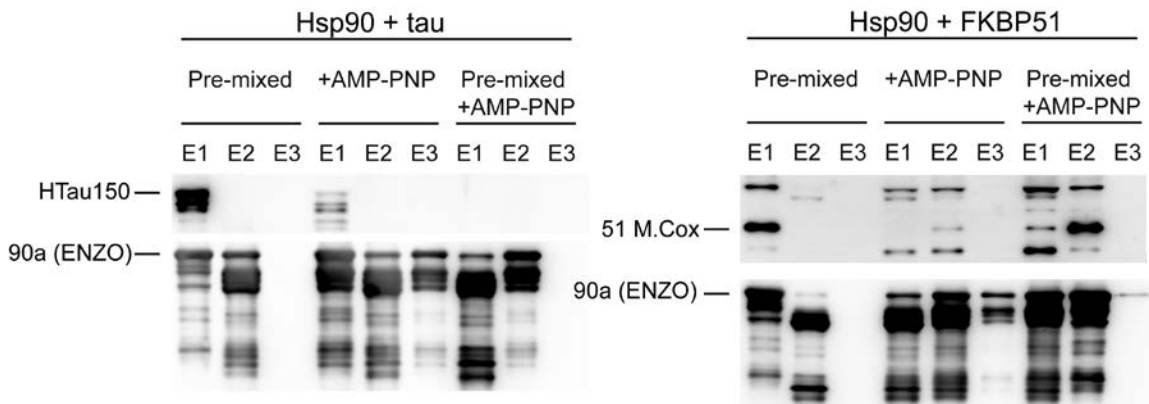


Figure 28. Western blot results of tau and FKBP51 binding to 6X His-tagged Hsp90. E1, E2, and E3 represent the three elution fractions collected after the elution step. 5 μ g of total protein was loaded in each well and run against antibodies for tau (HTau150), FKBP51 (51 M. Cox) and Hsp90 α (90a ENZO) (Byrd Alzheimer's Institute, Tampa, FL). Pre-mixed denotes protein samples that were pre-mixed for 30 minutes at 25°C prior to application to the mini column. Fractions with

+AMP-PNP indicates samples of Hsp90 that were incubated with AMP-PNP (a non-hydrolyzable version of ATP) for 30 minutes prior to application to the mini column.

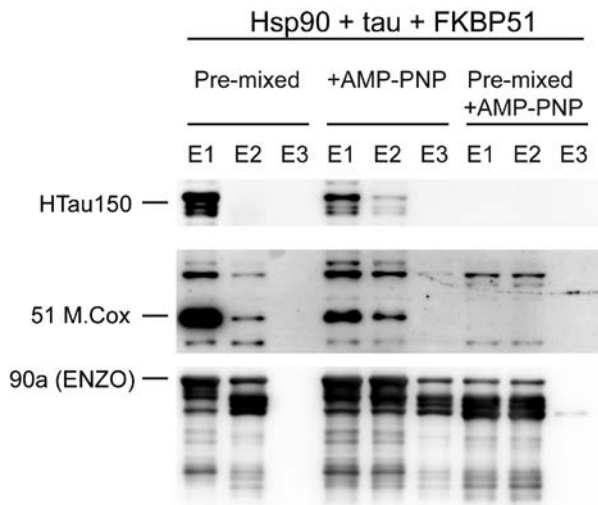


Figure 29. Western blot results of ternary complex formation for Hsp90, FKBP51 and tau. E1, E2, and E3 represent the three elution fractions collected after the elution step. 5 µg of total protein was loaded in each well and run against antibodies for tau (HTau150), FKBP51 (51 M. Cox) and Hsp90α (90a ENZO) (Byrd Alzheimer's Institute, Tampa, FL). Pre-mixed denotes

protein samples that were pre-mixed for 30 minutes at 25°C prior to application to the mini column. Fractions with +AMP-PNP indicate samples of Hsp90 that were incubated with AMP-PNP (a non-hydrolyzable version of ATP) for 30 minutes prior to application to the mini column.

Fractions analyzed by SDS-PAGE were of too low resolution to detect the quantities of proteins present in the fractions. Therefore, western blotting was performed on the same fractions probing with respective antibodies for Hsp90, tau, and FKBP51. The results demonstrate that tau and FKBP51 are able to associate with Hsp90 immobilized to Cobalt resin, both alone, and in the presence of one another. AMP-PNP was added in one round of experiments in an attempt to keep the Hsp90 dimer in an open conformation, however; it appears that when AMP-PNP is present there is a slight decrease in the association of tau and FKBP51 with Hsp90. This effect is further magnified when Hsp90 is incubated with AMP-PNP prior to application to the column, completely knocking out tau's association with Hsp90 over the column, as shown in Figure

28. It is likely that in order for tau to associate with the co-chaperone complex, Hsp90 must first bind FKBP51, thereby altering its conformation and promoting the association of Hsp90 with tau.

Model of the Hsp90-FKBP51 complex

Based on the binding studies presented here and previous work on the interaction between tau, Hsp90, and FKBP51 [45,67,85,88,89], we are able to propose a structural model for the Hsp90-FKBP51 complex. It is known that the C-terminal TPR domain of FKBP51 will interact with the MEEVD sequence that is at the C-terminus of Hsp90. Using this minimal constraint as a starting point, the initial structures of FKBP51 and Hsp90 were taken from the RCSB Protein Data Bank, files 1KT0 and 2CG9, respectively [7,8,90]. From here, we manually created new PDB files from the previously existing files to place Hsp90 and FKBP51 in the context of one another *in silico*. Perhaps the most interesting observation between the crystal structures of these two proteins is the apparent complementary interface that exists between Hsp90 and FKBP51. This combined with the previous knowledge regarding the TPR domain of Hsp90 allowed us to manually orient the crystal structures in a way that the two interaction domains (TPR and MEEVD recognition site) would be within proximity to one another. This natural orientation also places the FK1 and FK2 domains of a single FKBP51 molecule near the bifurcated cleft formed by the Hsp90 dimer. Given these considerations, an initial docking procedure using custom scripts (see Methods for full description simulation parameters) was performed using the

crystal structure of the closed form of human Hsp90 and the crystal structure of FKBP51.

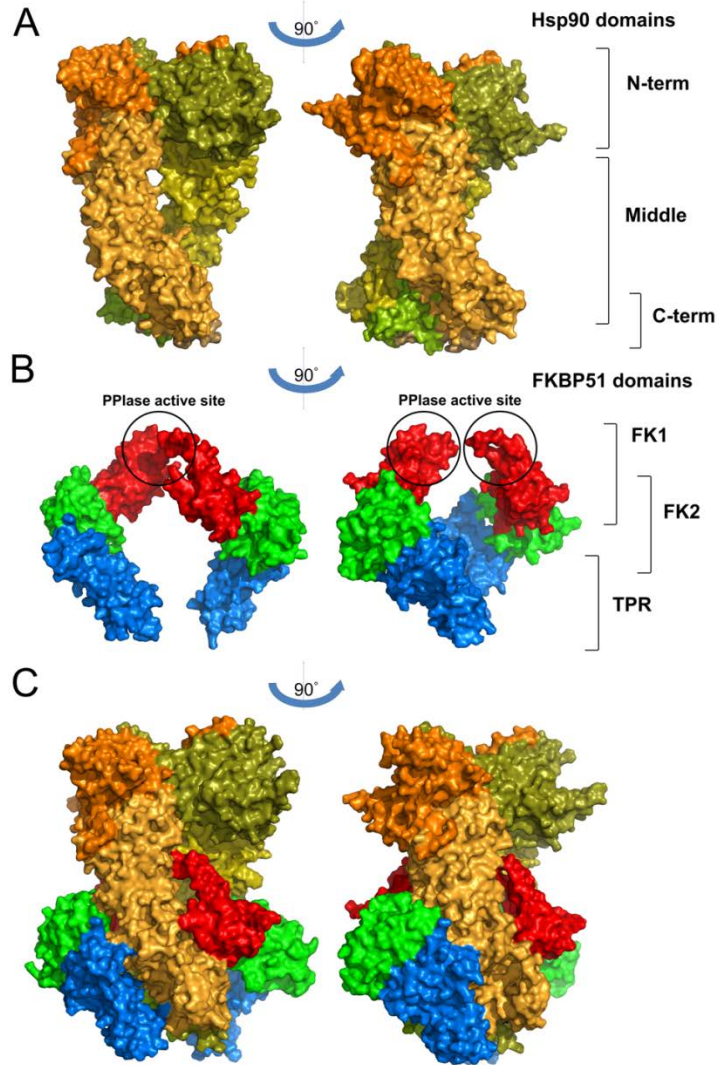


Figure 30. Structures of the Hsp90, FKBP51 and proposed FKBP51-Hsp90 complex. (A) Domain structure of human Hsp90 homodimer showing domain boundaries. Colors correspond to the domain boundaries for each of the main monomer subunits. (B) Structure of two FKBP51 subunits aligned in 3D to fit Hsp90 homodimer at binding positions proposed in this study. FK1, FK2 and TPR domains are highlighted in red, green and blue, respectively. The PPIase binding site in FK1 domain is outlined with black circles. (C) Structure of the proposed Hsp90-FKBP51 complex after 100ns of MD simulation. The figure was prepared using Pymol [57]. (Hsp90 PDB ID: 2CG9, FKBP51 PDB ID: 1KT0)

Using VMD for visualization, solvent accessible surfaces of both Hsp90 and FKBP51 were used to define limiting boundaries for intermolecular steric clashes [91,92]. The crystal structure of the closed form of Hsp90 without the Sba1 co-chaperone proteins is presented in Figure 30A [8]. Figure 30A also highlights the domains of the Hsp90 homodimer with different colors. As mentioned previously, the two middle domain subunits of Hsp90 form a bifurcated cleft when Hsp90 is in the closed conformation. This surface topology, combined with knowledge that the C-terminal TPR domain of FKBP51 interacts with the C-terminal dimerization domain of Hsp90, suggests a possible orientation for FKBP51 relative to Hsp90 where two molecules of FKBP51 fit into the concentric groove that wraps around the two Hsp90 subunits and ends at the bifurcated cleft. In Figure 30B, two FKBP51 molecules are shown in an orientation where they fit into the groove on Hsp90.

Monitoring the stability of the Hsp90 – FKBP51 complex

To determine whether the model for the Hsp90-FKBP51 complex was plausible, a 100 ns molecular dynamics (MD) simulation was performed (see Methods). A snapshot of the final structure from the 100 ns MD trajectory is shown in Figure 30C. The PPlase active sites from both FK1 domains are facing towards the binding pocket formed by the bifurcated cleft on the middle domains of Hsp90. Both the FK2 and TPR domains remain aligned along the surface of Hsp90. The model shows that the binding sites of the TPR domains are in close proximity to the C-terminal dimerization domains and the intrinsically disordered linker of the C-terminal domain. The intrinsically disordered linker and the C-

terminal MEEVD recognition site were not included in the model for two reasons. The first is the inherent uncertainty involved in modeling the disordered C-terminal tail of Hsp90. The second reason was to determine whether the apparent complementary interface between Hsp90 and FKBP51 was sufficient to keep the complex together during the simulation.

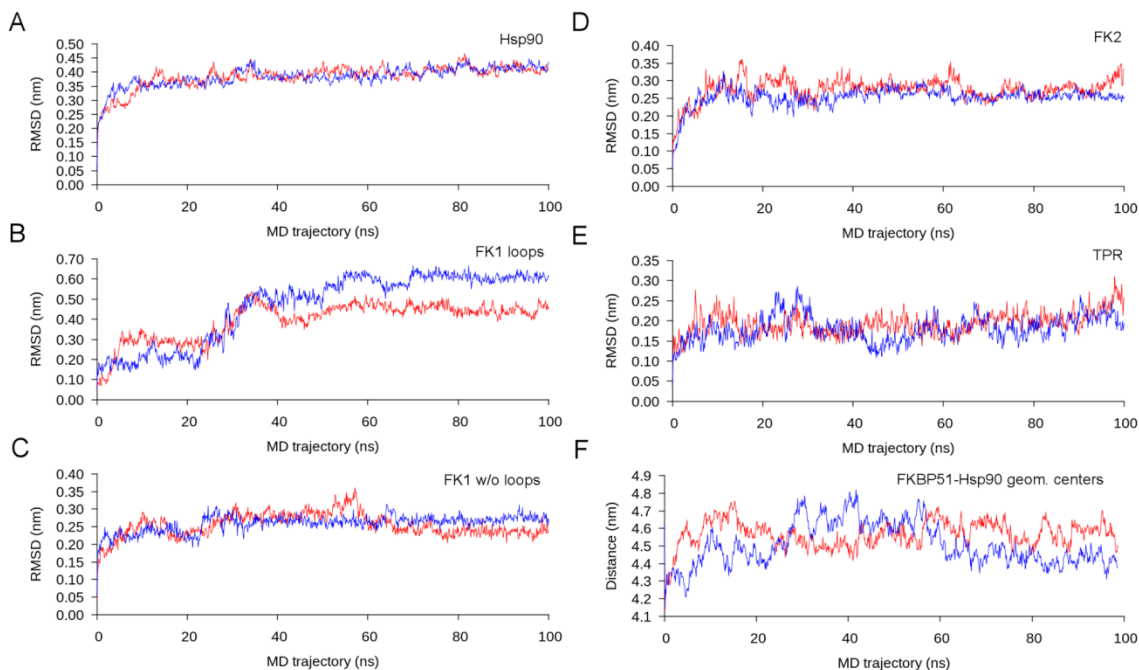


Figure 31. Plots of backbone RMSD and distances between geometric centers for the proposed Hsp90-FKBP51 complex model. Red and blue lines indicate individual monomers of Hsp90 or FKBP51. (A) Backbone RMSD of two main monomeric units of Hsp90 heterodimer. (B) Backbone RMSD of loop regions in PPlase binding sites for two FK1 domains. (C) Backbone RMSD for two FK1 domains excluding the loop regions in PPlase binding sites. (D) Backbone RMSD of two FK2 domains. (E) Backbone RMSD of two TPR domains. (F) Distance between geometric centers of FKBP51 and geometric center of Hsp90 measured for each of two bound FKBP51 subunits.

Relevant distances were monitored over the course of the MD simulation to check the stability of the proposed model for the Hsp90-FKBP51 complex.

Some of these distances are plotted in Figure 31A. The root mean square difference (RMSD) in the position of the backbone atoms from the two subunits of Hsp90 is shown in Figure 31A. This figure shows that the RMSD of the backbone atoms for both Hsp90 subunits reaches an equilibrium value of less than 4 Å in the first 20 ns of the simulation.

The FK1 domain of FKBP51 contains a disordered loop region between residues 113 and 126 that forms part of the PPlase active site (see black circle in Figure 30B). Figure 31B shows that this loop region has the highest backbone RMSD values when compared with the backbone RMSD of remaining residues in FK1, which are shown in Figure 31C. In the model proposed for the Hsp90-FKBP51 complex, the loop region and the PPlase active site are facing the bifurcated cleft formed by the middle domain of Hsp90. The plot in Figure 31B demonstrates that the topology of the loops in both FK1 domains changes significantly with respect to the initial position in the PDB file. The backbone dynamics for these loops are stabilized at about 35 ns. Such behavior is driven by the interaction between these loops and the residues in the binding cleft of the middle domain of Hsp90, suggesting these loops are involved in forming a prominent interaction surface for the Hsp90-FKBP51 complex. The dynamics of the rest of the FK1 β -sheet backbone is quite rigid with similar backbone behavior observed in the FK2 and TPR domains, as shown in Figures 31D and 31E, respectively.

Figure 31F shows the distances between the geometric centers of each of FKBP51 subunit and the geometric center of the Hsp90 homodimer. The

distances for both FKBP51 subunits fluctuate by a couple of angstroms but are reasonably stable around a value of 46 Å after 25 ns. This highlights the fact that the FKBP51 subunits do not move apart from Hsp90 and emphasizes the mutually favorable interactions between FKBP51 and Hsp90. The RMSD and distance measurements presented in this section, along with the coordinates of the final structure from the 100 ns MD trajectory presented in Figure 30C, allows us to conclude that the model of the Hsp90-FKBP51 complex is reasonably stable.

CHAPTER FOUR: DISCUSSION

The interaction between the FK1 domain and FK506

The spectral analysis presented in chapter two presents an interesting case for the interaction between the FK1 domain of FKBP51 and tau. Firstly, it is curious that one of the most important residues in conferring PPlase activity, D68, experiences the most significant reduction in intensity upon addition of tau. In fact, studies on the PPlase activity in the FK1 regions have confirmed that D68 mutants of FK1 experience partial or total loss of PPlase activity [6]. When Bracher et al. determined the crystal structure of FK1 in 2011, they determined that upon binding to FK506, residues Y57, F67, D68, F77, and I87 shift sideways allowing for a wider entrance to the binding site [6]. These residues line the rim of the conserved FK506 binding pocket.

The interaction between the FK1 domain and tau

Interestingly, in our intensity ratio plots for ^{15}N -labeled FK1 in the presence of tau, residues Y57, D68, and I87 all experience significant intensity reductions either at or below one standard deviation from the mean (Y57 and F67 are unassigned). In our spectrum of ^{15}N -labeled FK1 in the presence of tau, the residue that experienced that largest chemical shift was I87. Furthermore, Bracher et al. determined that the backbone amide of I87 was hydrogen bonded in all higher resolution structures published for the FK1 domain, indicating that bonding at the I87 amide might be crucial for an interaction to take place [6].

Based on this evidence we can conclude that D68, F77, and I87 may assist in orienting the tau protein so that it may interact with the active site.

Upon examination of the crystal structure of FK1 bound to FK506 it is clear that several of the resonances that we see experience changes in the presence of tau also contribute to the largest intermolecular forces present in the binding pocket of the crystal structure. In particular hydrogen bonding between residues D68, I87, Q85 and Y113 contribute greatly to the strength of the interaction between FK1 and FK506 [6]. Our intensity ratio plots presented in Figure 15 also demonstrate that D68, I87, Q85 all experience significant intensity reductions in the presence of tau and we can reasonably conclude that these strong intermolecular forces are contributing to a weak interaction between FK1 and tau.

Regions that we showed to form strong beta-sheet structure experienced average changes in intensity. The strong beta-sheet topology surrounding a central helix on FK1 alone was also confirmed using HNCACB experiments. The residues in the HSQC spectra of FK1 that experienced the largest changes in intensity upon addition of tau also fall within regions that correspond to beta-sheet structure.

Tau associates with Hsp90 and FKBP51 using two C-terminal hexapeptide motifs

Using NMR spectroscopy, MD simulations, and other biochemical techniques we have been able to further characterize tau's interaction with Hsp90 and FKBP51 [45,67,88]. The NMR titrations presented in chapter three

between ¹⁵N-labeled tau, Hsp90, and FKBP51 provide the first structural assessment of the interaction and demonstrate that tau's hexapeptide motifs form overlapping binding sites for Hsp90 and FKBP51. Previous evidence regarding the progression of an Hsp90 co-chaperone complex containing FKBP51 through the reaction cycle of ATP binding, hydrolysis, and release, showed that the presence of varying stoichiometries of co-chaperones can alter association of the complex with client proteins [88]. It is likely that the system described here comprised of Hsp90, FKBP51 and tau is missing other co-chaperones that may be needed to alter Hsp90's conformation and promote client association/dissociation. This assumption is supported by previous studies demonstrating that mixed co-chaperone complexes (e.g. those containing Hsp90, PPlases and other co-chaperones such as p23) are required for the full progression of the Hsp90 reaction cycle [67,88,89].

It is normal for client and co-chaperone proteins to elicit competitive binding to various domains of Hsp90 [93]. It is difficult to infer the extent of competitive binding going on between Hsp90 and FKBP51 along the hexapeptide regions. This may be partly due to the homology between the two hexapeptide regions and the dynamic nature of full-length tau. Taking this into account, it is possible that tau could be bound to the co-chaperone complex in such a way that each hexapeptide region associates independently with either Hsp90 or FKBP51. The fact that Hsp90 and FKBP51 bind to overlapping sites on tau also suggests a possible model for ternary complex formation where Hsp90 localizes tau so that it can interact with the PPlase domain of FKBP51. Closer examination of

Figures 25A and 25B suggests that the interaction between Hsp90 and tau is probably stronger at residues V306 – K311 than that of tau with FKBP51 in the same region. This conclusion is based on the magnitude and extent of the resonance intensity reductions for residues V306 – K311 versus residues V275 – K280. This is consistent with a previous study showing that tau needs the hexapeptide V306 – K311 in order to interact with Hsp90 via co-immunoprecipitation. This study was able to measure the association of tau's hexapeptide regions with Hsp90 and concluded that Hsp90 can mediate a conformational change in the tau protein upon association [85]. Conversely, Figure 25B shows a stronger interaction between tau and FKBP51 in the hexapeptide V275 – K280. In terms of tau biology, these hexapeptides can form the highest amount of transient secondary structure in full length tau and are important for binding to Hsp90 [24,94]. The formation of transient beta-sheet structure is necessary for tau to aggregate and form paired helical filaments - the precursors to neurofibrillary tangle formation in the brain [24,94]. Mandelkow et al. has also shown that mutations in the hexapeptide regions promote tau aggregation [86].

Possible model of the Hsp90-FKBP51 co-chaperone complex

Based on previous observations regarding the Hsp90-FKBP51 co-chaperone complex and the NMR data presented here, a computational model simulating the Hsp90-FKBP51 complex was constructed [67,88,89]. MD simulations performed on this model demonstrate the complex is stable over a 100 ns timescale and that there are no strong, unfavorable intermolecular forces

hindering the interaction. This is an important fact because it illustrates that it is at least possible for the complex to stay together. Although the TPR domain is important for the interaction between FKBP51 and Hsp90, it is not the only domain that facilitates the interaction. Previous co-immunoprecipitation studies have demonstrated that the FK domains (FK1 and FK2) must be present in order for FKBP51 to bind Hsp90 [66]. The computational model presented in Figure 30 highlights the favorable interaction surface between the FK domains of FKBP51 and Hsp90.

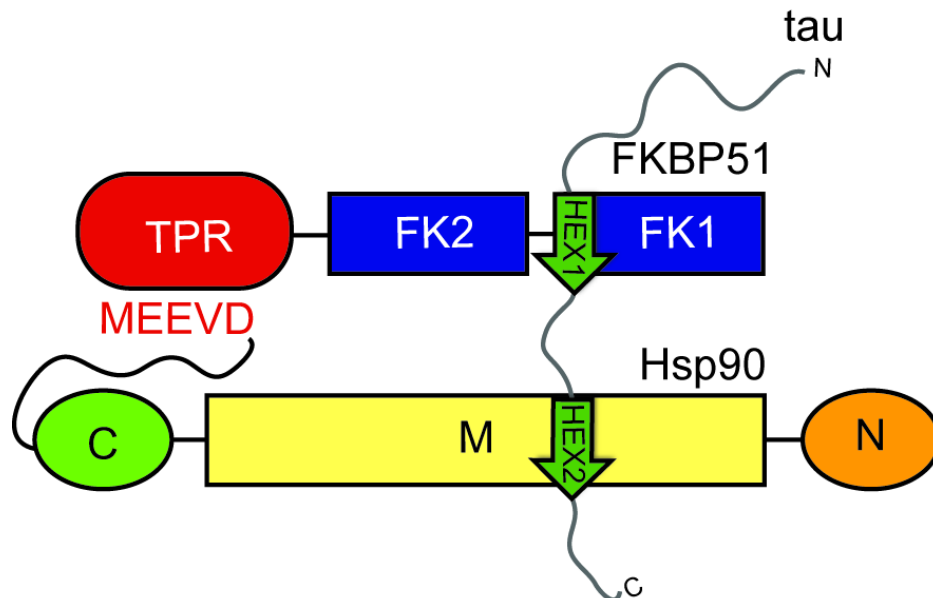


Figure 32. Cartoon model of tau's interaction with the Hsp90 – FKBP51 complex. HEX 1 and HEX 2 correspond to hexapeptide V275 – K280 and hexapeptide V306 – K311, respectively. Cartoon proposes a possible orientation where tau can interaction with FKBP51 and Hsp90 along HEX1 and HEX 2, respectively.

In terms of the model presented in Figure 30, it is also important to note that the PPIase active site of the FK1 domain on FKBP51 is facing the bifurcated cleft formed by the Hsp90 homodimer, as shown in Figures 30B and 30C.

Looking more closely at the RMSD plots in Figure 31 it was noted that this loop region comprising residues 113-126 in the PPlase region on the FK1 domain, undergoes significant changes during the simulation upon interaction with the bifurcated cleft formed by the two middle domains of the Hsp90 dimer. We propose that this natural cleft may be a favorable site for tau to simultaneously bind Hsp90 and FKBP51, supporting a model for ternary complex formation where Hsp90 localizes tau so that it may interact with the PPlase domain of FKBP51. A cartoon model of this proposed interaction is presented in Figure 32. This has also been partially supported by our NMR data demonstrating that specific residues in the PPlase active site undergo changes in the presence of tau.

Determining precisely how tau's behavior is regulated in the brain will help us to further understand how protein-protein interactions and post-translational modifications along the way can lead to unregulated misfolding and aggregation of tau into tangles. Hsp90 is abundant in the brain and this study has succeeded in identifying specific regions on tau capable of interacting with Hsp90 and its co-chaperone, FKBP51. Understanding how co-chaperones like FKBP51 interplay with Hsp90 is another piece of the tau regulation puzzle that is not quite clear but is ever emerging. Tau's association with these complexes is important because the association of these proteins will ultimately regulate how and when tau is degraded. Unraveling the mechanism behind how alterations to tau's degradation pathway affect normal protein homeostasis continues to be a major focal point of research studies on neurodegenerative disorders.

CHAPTER FIVE: MATERIALS AND METHODS

Protein expression

All proteins were expressed in the pET-28a vector system carrying genes for wild-type 0N4R tau (molecular mass 42,000.7 Da, 383 a.a.), Hsp90 α (molecular mass 86,323.4 Da, 732 a.a.) and FKBP51 (molecular mass 52,212.2 Da, 457 a.a.). Plasmids for full length 0N4R tau, Hsp90 α , FKBP51 and were provided by Dr. Chad Dickey (Byrd Alzheimer's Institute, Tampa, FL). Original vectors were modified via mutagenesis to include a TEV protease site prior to the N-terminus of the tau gene and a PreScission protease site prior to the N-terminus of the FKBP51 gene. FK1 (15,168 Da, 138 a.a.) constructs were obtained from GeneArt (Invitrogen, Grand Island, NY) in a pUC vector and subsequently cloned into a pET-28a vector including a 6XHis tag. All plasmids were transformed into *Escherichia coli* strain BL21 (DE3). All tau, FKBP51, and FK1 protein expression was performed at 37°C in M9 minimal media which allows for efficient metabolic incorporation of isotope labels such as ^{15}N and ^{13}C by using $^{15}\text{NH}_4\text{Cl}$ and ^{13}C D-Glucose. Hsp90 α expression was also done in M9 minimal media, however; induction was carried out at 18°C for 20hrs to achieve optimal expression levels. For all proteins, expression was induced at OD 0.8 by addition of 1mM isopropyl- β -D-thiogalactopyranoside (IPTG) to 2L culture flasks, grown for 4 - 20 hours, pelleted via centrifugation at 8000 rpm for 15 min. at 4°C

and stored at -80°C. The recipe for M9 media can be found in the Methods section under the subheading 'Buffer Recipes'.

Protein purification

Cell pellets were thawed and re-suspended in a PBS buffer containing 10mM Imidazole, 100µM PMSF and P2174 (10X) protease inhibitor cocktail from Sigma Aldrich. Cells were lysed via French Press at $\geq 20,000$ psi. The lysate was separated via centrifugation at 18,000 rpm for 1 hour at 4°C. The clarified lysate was loaded onto a column containing HisPur™ cobalt resin (Thermo Scientific, West Palm Beach, FL). Prior to purification, the resin was equilibrated with 50 mM NaH₂PO₄, 300 mM NaCl, 10 mM Imidazole, 0.02% NaN₃, 4 mM DTT, pH 7.4 and eluted with 150 mM Imidazole. The Histidine tag was cleaved using TEV or HRV3C proteases and separated from the untagged protein using a column containing HisPur™ cobalt resin. Cleaved proteins were then dialyzed into a gel filtration buffer (50 mM NaH₂PO₄, 300 mM NaCl, 1 mM EDTA, 0.02% NaN₃, pH 7.0) and loaded onto a HiLoad 16/60 Superdex 75 prep grade column (Pharmacia, 17 1068-01). All proteins were eluted with a flow rate of 0.35 or 1.0 mL/min, pooled and dialyzed into an appropriate buffer for NMR analysis, and finally concentrated to 2-15 mg/mL. All proteins were confirmed to be $\geq 90\%$ pure by Coomassie stained SDS-PAGE. The workflow for the purification of all proteins can be found in the Sample Preparation section of Chapters 2 and 3. Recipes for all media and buffers can be found in the Methods section under the subheading 'Buffer Recipes'.

Determining protein concentration

Proteins were concentrated using Milipore (Billerica, MA) centrifugal filter units with a 3,500 MWCO, spun at 3300 RCF. All protein concentrations were determined using a Nanodrop ND-1000 requiring 2 μ L of sample to conduct the assay. Absorbances were taken at 280 nm and are based on the presence of tryptophan, tyrosine and cysteine residues. Extinction coefficients were calculated using publically available software ProtParam from ExPASy and are listed below for all proteins.

Protein Reference Chart							
Protein	MW	w/o	tag	E.C.	Length	# of C	pl
	(KDa)			(M/cm)	(a.a.)	Residues	
<i>tau</i>	40000.7			7450	383	2	9.46
<i>Hsp90α</i>	84659.7			59250	732	7	4.94
<i>Hsp90β</i>	83264.2			57760	724	6	4.96
<i>FKBP51</i>	51212			40340	457	9	5.71
<i>FK1</i>	15168			11460	138	2	6.83

Figure 33. Protein reference chart. MW indicates the molecular weight in KDa of each protein of interest. E.C. stands for extinction coefficient, which is used to determine the final concentration of the protein. # of C residues denotes the numbers of cysteine residues present and pl denotes the isoelectric point of each protein.

NMR data acquisition

Experimental parameters

NMR experiments on tau were carried out at 298 K on a Varian VNMRs 800 MHz spectrometer equipped with a triple resonance pulse field Z-axis gradient cold probe. Resonance assignments for 0N4R tau were inferred using previous

assignments [24,84]. To make the amide ^1H and ^{15}N resonance assignments, sensitivity enhanced ^1H - ^{15}N HSQC were performed on the uniformly ^{15}N -labeled tau samples in 90% H_2O /10% D_2O , PBS buffer with 4mM DTT at a pH 6.0. For the HSQC experiments, data were acquired in ^1H and ^{15}N dimensions using 2100.0 (t_2) 9615.3846 (t_1) Hz sweep widths, and 1024 (t_2) 128 (t_1) complex data points. HNCACB experiment data were acquired in ^1H , ^{13}C and ^{15}N dimensions using 8012.8 (t_3) x 12000 (t_2) x 2000 (t_1) Hz sweep widths, and 1024 (t_3) x 128 (t_2) x 32 (t_1) complex data points. All NMR spectra were processed with nmrPipe and analyzed using nmrView [95]. The ^1H carrier frequency was set on the water peak, and 4.753 ppm was used as the reference frequency.

HSQC and HNCACB experiments

The heteronuclear single quantum coherence (HSQC) experiment is a two dimensional heteronuclear shift correlation experiments that can monitor how a spin is transferred between a proton and another bonded atom. In this case we are exploiting the fact that each residue of a protein (with the exception of proline) has an amide proton attached to nitrogen in the peptide bond. This experiment is designed such that a spin is transferred from the amide proton to the nitrogen and back again to yield a resonance for each non-proline residue of the protein. These experiments were primarily used in order to determine the change in chemical shifts and/or intensity changes for those residues involved in binding.

While the HSQC is a high resolution two dimensional NMR experiment correlating the ^1H and ^{15}N atoms, HNCACB experiments are three dimensional NMR experiments that can be used to assign all residues along the backbone of a protein of interest. The HNCACB requires the protein to have both magnetically labeled N, and C, and the experiments are designed such that the spin is transferred from the amide proton through the covalent bonds to the N, C_α and C_β atoms and back, yielding a signal that has resonances in the corresponding frequencies. This allows a spectra to be generated in three dimensions with the ^1H , ^{15}N , and ^{13}C making up the x, z, and y axis respectively. For the HNCACB there is also a weaker resonance coming from the previous residues' C atoms. This allows for the correlation of multiple spin system, generating a more high definition picture of the backbone of the protein.

Cobalt binding assay

Binding experiments were performed on cobalt His-Pur Resin (Thermo Scientific, West Palm Beach, FL) using mini 1mL columns obtained from Bio-Rad (Hercules, CA). 500 μL of a 50% resin slurry was spun down at 700 x g for 2 minutes and the supernatant was removed. Cobalt resin was washed with three bed volumes (750 μL) of cobalt A1 Buffer. 500 μL of a His-tagged protein (in Co A1) was applied to the resin and incubated at room temperature with gentle agitation for 30 minutes. Resin with bound protein was washed with three bed volumes of Co A1 to wash out any unbound sample. On the second wash the supernatant was removed and a 15 μL sample was taken for SDS-PAGE analysis. 1mL of non-tagged proteins were applied to the resin with bound

Hsp90, respectively. Tubes were incubated at room temperature with gentle agitation for 30 minutes. Resin was then washed with three bed volumes of Co A1. Samples of the supernatant and the resin were taken following centrifugation after the third wash. The His-tagged protein was eluted with 150mM Imidazole. 15 μ L samples were taken from the supernatant following elution. All samples were mixed with 15 μ L of 2x Lamelli Buffer and run on a 10% SDS-PAGE gel at 200V for 50 minutes.

Molecular dynamics simulation

All molecular dynamics simulations were performed over 100 ns using GROMACS 4.5 [96-98] with the AMBER99SB force field [99] in a periodic dodecahedron box with TIP3P water [100]. The nearest distance from the box edge was set to 1.2 nm. Ions were added to a concentration of 0.15 M to neutralize the system. 5000 steps of a steepest descent algorithm was used for energy minimization, with a tolerance of 1000 kJ/(mol/nm). After energy minimization, a 700 ps position restrained molecular dynamics simulation at constant volume (NVT) was performed to equilibrate the water molecules around the complex and stabilize temperature. The temperature (300 K) of the system was controlled with the Berendsen algorithm [101]. Afterward, an unrestrained molecular dynamics simulation of the system was carried out for 50 ns at constant pressure, and temperature (NPT). The temperature (300 K) and pressure (1 atm) of the simulation was controlled using the Nose-Hoover thermostat [102,103] and Parrinello-Rahman barostat, respectively [104]. The Lincs algorithm [105] was used to constrain all bonds to their equilibrium lengths, allowing a time step of 2 fs. Particle Mesh Ewald (PME) method [106] was applied for electrostatics with a real space cutoff of 0.8 nm, a grid spacing of 0.12 nm and cubic spline interpolation. The cutoff for non-bonded Van der Waals

interactions was set to 0.8 nm. A detailed experimental rationale is given in the Results and Discussion section under the subheading Model of the Hsp90-FKBP51 Complex.

Subcloning of GeneArt constructs

- Worktable for restriction digest of plasmid obtained from GeneArt to recover insert of interest or open new vector for cut and paste
- **Table 1. Worktable for restriction digestions.**

Reagent	Volume
<i>H₂O</i>	6 μ L
<i>NEB Buffer</i>	2 μ L
<i>GeneArt Plasmid/Vector</i>	10 μ L
<i>XhoI</i>	1 μ L
<i>EcoRI</i>	1 μ L
Total:	20μL

- Tubes gently mixed and incubated for 16h at 37⁰C at 250rpm.
- The digested plasmid sample is run on an agarose gel in order to separate the vector from the insert of interest. A gel extraction procedure is then performed using a OIAquick Gel Extraction Kit (Qiagen, Germantown, MD) in order to remove and purify the insert from the agarose gel.

Ligation of construct into vector of interest

- Once the insert of interest has been separated and purified from the pUC vector and the vector of interest (pET28a) has been digested, the two can be ligated together.
- **Table 2. Worktable for ligation reactions.**

Reagent	Mix 1	Mix 2
<i>10X T4 buffer</i>	2 μ L	2 μ L
<i>Vector DNA</i>	1 μ L	2 μ L
<i>Insert</i>	10 μ L	15 μ L
<i>H₂O</i>	6 μ L	0 μ L
<i>T4 ligase</i>	1 μ L	1 μ L
Total:	20 μL	20 μL

- Prepare two different reaction tubes according to the chart above and incubate overnight at 16^oC for 16h.

Transformation of newly ligated constructs

- Transform 2.5 μ l of each ligation reaction into NEB5 α cells. Plate the entire 100 μ l transformation reaction onto LB media with kanamycin. Incubate overnight at 37^oC for 18 to 22 hours.
- Inoculate 6ml NZY broth + kanamycin/ ampicillin with individual colonies from overnight plates. Incubate in shaker incubator at 37^oC for 16h.

- Extract plasmid using Qiagen Plasmid Miniprep Kit (Qiagen, Germantown, MD). Elute in 30 μ l EB buffer. Estimate plasmid concentration using the Nanodrop Spectrophotometer. Send 15 μ l to Operon (Eurofins MWG, Huntsville, AL) for sequencing.

Buffer Recipes

Preparation of M9 Minimal Media (2L):

Stock Solutions for M9

- 10X M9 Salts (1L)

Na ₂ HPO ₄	60g
KH ₂ PO ₄	30g
NaCl	5g
- 1M MgSO₄ Filter sterilized
- 20% Dextrose Filter sterilized
- 50mM CaCl₂ Filter sterilize
- 0.01 M FeCl₃
- 5mg/ml Vitamin B1

M9 Minimal Media:

- 200mL of 10x M9 salts
- 4mL 1M MgSO₄
- 20mL of 20% D-Glucose
- 4mL of 50mM CaCl₂
- 2mL 0.01M FeCl₃
- 400uL of 5mg/mL Vitamin B1
- pH to 7.3-7.5
- QS to 2L with ddH₂O

Preparation of Cobalt Column Buffers (1L):

Co A1 Buffer (Lysis/Binding)

- 50mM NaH₂PO₄
- 300mM NaCl
- 10mM Imidazole
- 0.02% NaN₃
- pH to 7.40

Co A2 Buffer (Wash)

- 50mM NaH₂PO₄
- 300mM NaCl
- 20mM Imidazole
- 0.02% NaN₃
- pH to 7.40

Co B Buffer (Elution)

- 50mM NaH₂PO₄
- 300mM NaCl
- 150mM Imidazole
- 0.02% NaN₃
- pH to 7.40

Preparation of Gel Filtration, NMR (1L):**Gel Filtration Buffer:**

- 50mM NaH₂PO₄
- 300mM NaCl
- 1mM EDTA
- 4mM DTT
- 0.02% NaN₃
- pH 7.00

NMR Buffer:

- 25mM NaH₂PO₄
- 100mM NaCl
- 1mM EDTA
- 4mM DTT
- 0.02% NaN₃

LITERATURE CITED

1. Weingarten MD, Lockwood AH, Hwo SY, Kirschner MW (1975) A protein factor essential for microtubule assembly. *Proc Natl Acad Sci U S A* 72: 1858-1862.
2. Tytell M, Brady ST, Lasek RJ (1984) Axonal transport of a subclass of tau proteins: evidence for the regional differentiation of microtubules in neurons. *Proc Natl Acad Sci U S A* 81: 1570-1574.
3. Wood JG, Mirra SS, Pollock NJ, Binder LI (1986) Neurofibrillary tangles of Alzheimer disease share antigenic determinants with the axonal microtubule-associated protein tau (tau). *Proc Natl Acad Sci U S A* 83: 4040-4043.
4. Gordon-Weeks PR (1991) Control of microtubule assembly in growth cones. *JCell SciSuppl* 15: 45-49.
5. Dosztányi Z, Csizmok V, Tompa P, Simon I (2005) IUPred: web server for the prediction of intrinsically unstructured regions of proteins based on estimated energy content. *Bioinformatics* 21: 3433-3434.
6. Bracher A, Kozany C, Thost AK, Hausch F (2011) Structural characterization of the PPlase domain of FKBP51, a cochaperone of human Hsp90. *Acta Crystallographica Section D: Biological Crystallography* 67: 549-559.
7. Sinars CR, Cheung-Flynn J, Rimerman RA, Scammell JG, Smith DF, et al. (2003) Structure of the large FK506-binding protein FKBP51, an Hsp90-binding protein and a component of steroid receptor complexes. *Proc Natl Acad Sci U S A* 100: 868-873.
8. Ali MMU, Roe SM, Vaughan CK, Meyer P, Panaretou B, et al. (2006) Crystal structure of an Hsp90–nucleotide–p23/Sba1 closed chaperone complex. *Nature* 440: 1013-1017.
9. IHARA Y, NUKINA N, MIURA R, OGAWARA M (1986) Phosphorylated tau protein is integrated into paired helical filaments in Alzheimer's disease. *Journal of biochemistry* 99: 1807-1810.
10. Kosik KS, Joachim CL, Selkoe DJ (1986) Microtubule-associated protein tau (tau) is a major antigenic component of paired helical filaments in Alzheimer disease. *Proceedings of the National Academy of Sciences* 83: 4044-4048.

11. Grundke-Iqbal I, Iqbal K, Tung Y-C, Quinlan M, Wisniewski HM, et al. (1986) Abnormal phosphorylation of the microtubule-associated protein tau (tau) in Alzheimer cytoskeletal pathology. *Proceedings of the National Academy of Sciences* 83: 4913-4917.
12. Baner C, Lassmann H, Budka H, Grundke-Iqbal I, Iqbal K, et al. (1987) Neurofibrillary tangles in Alzheimer's disease and progressive supranuclear palsy: antigenic similarities and differences. Microtubule-associated protein tau antigenicity is prominent in all types of tangles. *Acta neuropathologica* 74: 39-46.
13. Goedert M, Spillantini M, Jakes R, Rutherford D, Crowther R (1989) Multiple isoforms of human microtubule-associated protein tau: sequences and localization in neurofibrillary tangles of Alzheimer's disease. *Neuron* 3: 519-526.
14. Arriagada PV, Growdon JH, Hedley-Whyte ET, Hyman BT (1992) Neurofibrillary tangles but not senile plaques parallel duration and severity of Alzheimer's disease. *Neurology* 42: 631-631.
15. Hutton M, Lendon CL, Rizzu P, Baker M, Froelich S, et al. (1998) Association of missense and 5'-splice-site mutations in tau with the inherited dementia FTDP-17. *Nature* 393: 702-705.
16. Spillantini MG, Murrell JR, Goedert M, Farlow MR, Klug A, et al. (1998) Mutation in the tau gene in familial multiple system tauopathy with presenile dementia. *Proc Natl Acad Sci U S A* 95: 7737-7741.
17. Hardy J, Orr H (2006) The genetics of neurodegenerative diseases. *J Neurochem* 97: 1690-1699.
18. Uversky VN, Oldfield CJ, Dunker AK (2008) Intrinsically disordered proteins in human diseases: introducing the D2 concept. *Annu Rev Biophys* 37: 215-246.
19. Prodromou C, Siligardi G, O'Brien R, Woolfson DN, Regan L, et al. (1999) Regulation of Hsp90 ATPase activity by tetratricopeptide repeat (TPR)-domain co-chaperones. *EMBO J* 18: 754-762.
20. Pearl LH, Prodromou C (2006) Structure and mechanism of the Hsp90 molecular chaperone machinery. *Annu Rev Biochem* 75: 271-294.
21. Wandinger SK, Richter K, Buchner J (2008) The Hsp90 chaperone machinery. *Journal of Biological Chemistry* 283: 18473-18477.
22. Murrell J, Koller D, Foroud T, Goedert M, Spillantini M, et al. (1997) Familial multiple-system tauopathy with presenile dementia is localized to

- chromosome 17. *The American Journal of Human Genetics* 61: 1131-1138.
23. Gustke N, Trinczek B, Biernat J, Mandelkow EM, Mandelkow E (1994) Domains of tau protein and interactions with microtubules. *Biochemistry* 33: 9511-9522.
 24. Mukrasch MD, Bibow S, Korukottu J, Jeganathan S, Biernat J, et al. (2009) Structural polymorphism of 441-residue tau at single residue resolution. *PLoS Biol* 7: e1000034.
 25. Trinczek B, Biernat J, Baumann K, Mandelkow E, Mandelkow E (1995) Domains of tau protein, differential phosphorylation, and dynamic instability of microtubules. *Mol Biol Cell* 6: 1887.
 26. Dumanchin C, Camuzat A, Campion D, Verpillat P, Hannequin D, et al. (1998) Segregation of a missense mutation in the microtubule-associated protein tau gene with familial frontotemporal dementia and parkinsonism. *Hum Mol Genet* 7: 1825-1829.
 27. Uversky VN (2003) What does it mean to be natively unfolded? *European Journal of Biochemistry* 269: 2-12.
 28. Uversky VN (2009) Natively unfolded proteins: a point where biology waits for physics. *Protein Science* 11: 739-756.
 29. Romero P, Obradovic Z, Li X, Garner EC, Brown CJ, et al. (2001) Sequence complexity of disordered protein. *Proteins: Structure, Function, and Bioinformatics* 42: 38-48.
 30. Dyson HJ, Wright PE (2002) Coupling of folding and binding for unstructured proteins. *Current opinion in structural biology* 12: 54.
 31. Dyson HJ, Wright PE (2005) Intrinsically unstructured proteins and their functions. *Nature Reviews Molecular Cell Biology* 6: 197-208.
 32. Plaxco KW, Gross M (1997) The importance of being unfolded. *Nature* 386: 657-659.
 33. Daughdrill GW, Narayanaswami P, Gilmore SH, Belczyk A, Brown CJ (2007) Dynamic behavior of an intrinsically unstructured linker domain is conserved in the face of negligible amino acid sequence conservation. *Journal of molecular evolution* 65: 277-288.
 34. Cheng Y, LeGall T, Oldfield CJ, Mueller JP, Van Y-YJ, et al. (2006) Rational drug design via intrinsically disordered protein. *Trends in biotechnology* 24: 435-442.

35. Demchenko AP (2001) Recognition between flexible protein molecules: induced and assisted folding. *Journal of molecular recognition* 14: 42-61.
36. Uversky V (2003) Protein folding revisited. A polypeptide chain at the folding–misfolding–nonfolding cross-roads: which way to go? *Cell Mol Life Sci* 60: 1852-1871.
37. Iakoucheva LM, Brown CJ, Lawson JD, Obradovic Z, Dunker AK (2002) Intrinsic disorder in cell-signaling and cancer-associated proteins. *Journal of molecular biology* 323: 573-584.
38. Mocanu MM, Nissen A, Eckermann K, Khlistunova I, Biernat J, et al. (2008) The potential for β -structure in the repeat domain of tau protein determines aggregation, synaptic decay, neuronal loss, and coassembly with endogenous Tau in inducible mouse models of tauopathy. *J Neurosci* 28: 737-748.
39. Voss K, Koren J, Dickey CA (2011) The Earliest Tau Dysfunction in Alzheimer's Disease? Tau Phosphorylated at S422 as a Toxic Seed. *American Journal of Pathology*, The 179: 2148-2151.
40. Iqbal K, Liu F, Gong CX, Alonso AC, Grundke-Iqbal I (2009) Mechanisms of tau-induced neurodegeneration. *Acta neuropathologica* 118: 53-69.
41. Hutton M, Lewis J, Dickson D, Yen S-H, McGowan E (2001) Analysis of tauopathies with transgenic mice. *Trends in molecular medicine* 7: 467-470.
42. Leclerc S, Garnier M, Hoessel R, Marko D, Bibb JA, et al. (2001) Indirubins inhibit glycogen synthase kinase-3 β and CDK5/P25, two protein kinases involved in abnormal tau phosphorylation in Alzheimer's disease. *Journal of Biological Chemistry* 276: 251-260.
43. Mazanetz MP, Fischer PM (2007) Untangling tau hyperphosphorylation in drug design for neurodegenerative diseases. *Nature Reviews Drug Discovery* 6: 464-479.
44. Baumann K, Mandelkow E-M, Biernat J, Piwnica-Worms H, Mandelkow E (1993) Abnormal Alzheimer-like phosphorylation of tau-protein by cyclin-dependent kinases cdk2 and cdk5. *FEBS letters* 336: 417-424.
45. Jinwal UK, Koren III J, Borysov SI, Schmid AB, Abisambra JF, et al. (2010) The Hsp90 cochaperone, FKBP51, increases Tau stability and polymerizes microtubules. *J Neurosci* 30: 591-599.
46. Ellis RJ, van der Vies SM (1991) Molecular chaperones. *Annual review of biochemistry* 60: 321-347.

47. Freeman BC, Morimoto RI (1996) The human cytosolic molecular chaperones hsp90, hsp70 (hsc70) and hdj-1 have distinct roles in recognition of a non-native protein and protein refolding. *The EMBO journal* 15: 2969.
48. Hartl FU (1996) Molecular chaperones in cellular protein folding.
49. Dou F, Netzer WJ, Tanemura K, Li F, Hartl FU, et al. (2003) Chaperones increase association of tau protein with microtubules. *Proceedings of the National Academy of Sciences* 100: 721-726.
50. Luo W, Dou F, Rodina A, Chip S, Kim J, et al. (2007) Roles of heat-shock protein 90 in maintaining and facilitating the neurodegenerative phenotype in tauopathies. *Proc Natl Acad Sci U S A* 104: 9511-9516.
51. Shimura H, Miura-Shimura Y, Kosik KS (2004) Binding of tau to heat shock protein 27 leads to decreased concentration of hyperphosphorylated tau and enhanced cell survival. *J Biol Chem* 279: 17957-17962.
52. O'Leary JC, Dharia S, Blair LJ, Brady S, Johnson AG, et al. (2011) A new anti-depressive strategy for the elderly: ablation of FKBP5/FKBP51. *PLoS one* 6: e24840.
53. Hideaki I, Yohtalou T, Yoshinobu E, Riki O (1993) Localization of HSP90 in rat brain. *International journal of biochemistry* 25: 93-99.
54. DeZwaan DC, Freeman BC (2008) HSP90: The Rosetta stone for cellular protein dynamics? *Cell Cycle* 7: 1006-1012.
55. Johnson JL, Brown C (2009) Plasticity of the Hsp90 chaperone machine in divergent eukaryotic organisms. *Cell Stress Chaperones* 14: 83-94.
56. Watson D (1991) Regional variation in the abundance of axonal cytoskeletal proteins. *Journal of neuroscience research* 30: 226-231.
57. DeLano WL (2002) The PyMOL molecular graphics system.
58. Brillantes A, Ondrias K, Scott A, Kobrinsky E, Ondriasová E, et al. (1994) Stabilization of calcium release channel (ryanodine receptor) function by FK506-binding protein. *Cell* 77: 513.
59. Siekierka JJ, Hung SH, Poe M, Lin CS, Sigal NH (1989) A cytosolic binding protein for the immunosuppressant FK506 has peptidyl-prolyl isomerase activity but is distinct from cyclophilin.
60. Fischer G, Wittmann-Liebold B, Lang K, Kiefhaber T, Schmid FX (1989) Cyclophilin and peptidyl-prolyl cis-trans isomerase are probably identical proteins.

61. Takahashi N, Hayano T, Suzuki M (1989) Peptidyl-prolyl cis-trans isomerase is the cyclosporin A-binding protein cyclophilin. *Nature* 337: 473-475.
62. Fischer S, Michnick S, Karplus M (1993) A mechanism for rotamase catalysis by the FK506 binding protein (FKBP). *Biochemistry* 32: 13830-13837.
63. Lu P-J, Wulf G, Zhou XZ, Davies P, Lu KP (1999) The prolyl isomerase Pin1 restores the function of Alzheimer-associated phosphorylated tau protein. *Nature* 399: 784-788.
64. Zhou XZ, Kops O, Werner A, Lu P-J, Shen M, et al. (2000) Pin1-dependent prolyl isomerization regulates dephosphorylation of Cdc25C and tau proteins. *Molecular cell* 6: 873.
65. Dickey CA, Koren J, Zhang YJ, Xu Y, Jinwal UK, et al. (2008) Akt and CHIP coregulate tau degradation through coordinated interactions. *Proceedings of the National Academy of Sciences* 105: 3622.
66. Barent RL, Nair SC, Carr DC, Ruan Y, Rimerman RA, et al. (1998) Analysis of FKBP51/FKBP52 chimeras and mutants for Hsp90 binding and association with progesterone receptor complexes. *Mol Endo* 12: 342-354.
67. Pirkl F, Buchner J (2001) Functional analysis of the hsp90-associated human peptidyl prolyl Cis/Trans isomerases FKBP51, FKBP52 and cyp40. *J Mol Biol* 308: 795-806.
68. Dickey CA, Kamal A, Lundgren K, Klosak N, Bailey RM, et al. (2007) The high-affinity HSP90-CHIP complex recognizes and selectively degrades phosphorylated tau client proteins. *J Clin Invest* 117: 648-658.
69. Owens-Grillo JK, Czar MJ, Hutchison KA, Hoffmann K, Perdew GH, et al. (1996) A model of protein targeting mediated by immunophilins and other proteins that bind to hsp90 via tetratricopeptide repeat domains. *Journal of Biological Chemistry* 271: 13468-13475.
70. Tai PKK, Chang H, Albers MW, Schreiber SL, Toft DO, et al. (1993) P59 (FK506 binding protein 59) interaction with heat shock proteins is highly conserved and may involve proteins other than steroid receptors. *Biochemistry* 32: 8842-8847.
71. Gold BG (2000) Neuroimmunophilin ligands: evaluation of their therapeutic potential for the treatment of neurological disorders. *Expert opinion on investigational drugs* 9: 2331-2342.
72. Snyder SH, Sabatini DM, Lai MM, Steiner JP, Hamilton GS, et al. (1998) Neural actions of immunophilin ligands. *Trends in pharmacological sciences* 19: 21-25.

73. Nair SC, Rimerman RA, Toran EJ, Chen S, Prapapanich V, et al. (1997) Molecular cloning of human FKBP51 and comparisons of immunophilin interactions with Hsp90 and progesterone receptor. *Molecular and cellular biology* 17: 594-603.
74. Schwarzingler S, Kroon GJ, Foss TR, Chung J, Wright PE, et al. (2001) Sequence-dependent correction of random coil NMR chemical shifts. *Journal of the American Chemical Society* 123: 2970-2978.
75. Kay LE (1993) Pulsed-field gradient-enhanced three-dimensional NMR experiment for correlating ^{13}C . α ./ β ., $^{13}\text{C}'$, and ^1H . α . chemical shifts in uniformly carbon-13-labeled proteins dissolved in water. *Journal of the American Chemical Society* 115: 2055-2057.
76. Zuiderweg ERP (2002) Mapping protein-protein interactions in solution by NMR spectroscopy. *Biochemistry* 41: 1-7.
77. Palmer AG, Grey MJ, Wang C (2005) Solution NMR spin relaxation methods for characterizing chemical exchange in high-molecular-weight systems. *Methods Enzymol* 394: 430-465.
78. Kleckner IR, Foster MP (2011) An introduction to NMR-based approaches for measuring protein dynamics. *Biochimica et Biophysica Acta (BBA)- Proteins & Proteomics* 1814: 942-968.
79. Dou F, Netzer WJ, Tanemura K, Li F, Hartl FU, et al. (2003) Chaperones increase association of tau protein with microtubules. *Proc Natl Acad Sci U S A* 100: 721-726.
80. Nemes Z, Devreese B, Steinert PM, Van Beeumen J, Fesus L (2004) Cross-linking of ubiquitin, HSP27, parkin, and alpha-synuclein by gamma-glutamyl-epsilon-lysine bonds in Alzheimer's neurofibrillary tangles. *Faseb J* 18: 1135-1137.
81. Petrucelli L, Dickson D, Kehoe K, Taylor J, Snyder H, et al. (2004) CHIP and Hsp70 regulate tau ubiquitination, degradation and aggregation. *Hum Mol Genet* 13: 703-714.
82. Shimura H, Schwartz D, Gygi SP, Kosik KS (2004) CHIP-Hsc70 complex ubiquitinates phosphorylated tau and enhances cell survival. *J Biol Chem* 279: 4869-4876.
83. Dickey CA, Dunmore J, Lu B, Wang JW, Lee WC, et al. (2006) HSP induction mediates selective clearance of tau phosphorylated at proline-directed Ser/Thr sites but not KXGS (MARK) sites. *Faseb J* 20: 753-755.

84. Kapitel V (2012) Untersuchung des Tau-Proteins mit Hilfe von NMR Spektroskopie [Dissertation]. Johann Wolfgang Goethe Universität: Johann Wolfgang Goethe Universität. 259 p.
85. Tortosa E, Santa-Maria I, Moreno F, Lim F, Perez M, et al. (2009) Binding of Hsp90 to tau promotes a conformational change and aggregation of tau protein. *J Alzheimers Dis* 17: 319-325.
86. von Bergen M, Barghorn S, Li L, Marx A, Biernat J, et al. (2001) Mutations of tau protein in frontotemporal dementia promote aggregation of paired helical filaments by enhancing local β -structure. *J Biol Chem* 276: 48165-48174.
87. Jeganathan S, von Bergen M, Brützlach H, Steinhoff HJ, Mandelkow E (2006) Global hairpin folding of tau in solution. *Biochemistry* 45: 2283-2293.
88. Li J, Richter K, Buchner J (2010) Mixed Hsp90-cochaperone complexes are important for the progression of the reaction cycle. *Nat Struct Mol Biol* 18: 61-66.
89. Richter K, Muschler P, Hainzl O, Reinstein J, Buchner J (2003) Sti1 is a non-competitive inhibitor of the Hsp90 ATPase. *J Biol Chem* 278: 10328-10333.
90. Berman HM, Westbrook J, Feng Z, Gilliland G, Bhat T, et al. (2000) The protein data bank. *Nucleic Acids Res* 28: 235-242.
91. Phillips JC, Braun R, Wang W, Gumbart J, Tajkhorshid E, et al. (2005) Scalable molecular dynamics with NAMD. *J Comput Chem* 26: 1781-1802.
92. Humphrey W, Dalke A, Schulten K (1996) VMD: visual molecular dynamics. *J Mol Graph* 14: 33-38.
93. Harst A, Lin H, Obermann WM (2005) Aha1 competes with Hop, p50 and p23 for binding to the molecular chaperone Hsp90 and contributes to kinase and hormone receptor activation. *Biochemical Journal* 387: 789.
94. Mukrasch MD, Biernat J, von Bergen M, Griesinger C, Mandelkow E, et al. (2005) Sites of tau important for aggregation populate β -structure and bind to microtubules and polyanions. *J Biol Chem* 280: 24978-24986.
95. Johnson BA, Blevins RA (1994) NMR View: A computer program for the visualization and analysis of NMR data. *J Biomol NMR* 4: 603-614.
96. Hess B, Kutzner C, van der Spoel D, Lindahl E (2008) GROMACS 4: Algorithms for highly efficient, load-balanced, and scalable molecular simulation. *J Chem Theory Comput* 4: 435-447.

97. Lindahl E, Hess B, Van Der Spoel D (2001) GROMACS 3.0: a package for molecular simulation and trajectory analysis. *J Mol Model* 7: 306-317.
98. Van Der Spoel D, Lindahl E, Hess B, Groenhof G, Mark AE, et al. (2005) GROMACS: fast, flexible, and free. *J Comput Chem* 26: 1701-1718.
99. Hornak V, Abel R, Okur A, Strockbine B, Roitberg A, et al. (2006) Comparison of multiple Amber force fields and development of improved protein backbone parameters. *Proteins* 65: 712-725.
100. Jorgensen WL, Chandrasekhar J, Madura JD, Impey RW, Klein ML (1983) Comparison of simple potential functions for simulating liquid water. *J Chem Phys* 79: 926.
101. Berendsen HJC, Postma JPM, van Gunsteren WF, DiNola A, Haak J (1984) Molecular dynamics with coupling to an external bath. *J Chem Phys* 81: 3684.
102. Nosé S (1984) A unified formulation of the constant temperature molecular dynamics methods. *J Chem Phys* 81: 511.
103. Hoover WG (1985) Canonical dynamics: Equilibrium phase-space distributions. *Phys Rev A* 31: 1695.
104. Parrinello M, Rahman A (1981) Polymorphic transitions in single crystals: A new molecular dynamics method. *J Appl Phys* 52: 7182-7190.
105. Hess B, Bekker H, Berendsen HJC, Fraaije JGEM (1997) LINCS: a linear constraint solver for molecular simulations. *J Comput Chem* 18: 1463-1472.
106. York DM, Darden TA, Pedersen LG (1993) The effect of long-range electrostatic interactions in simulations of macromolecular crystals: A comparison of the Ewald and truncated list methods. *J Chem Phys* 99: 8345.

APPENDICES

APPENDIX A: Dynamic Light Scattering Results

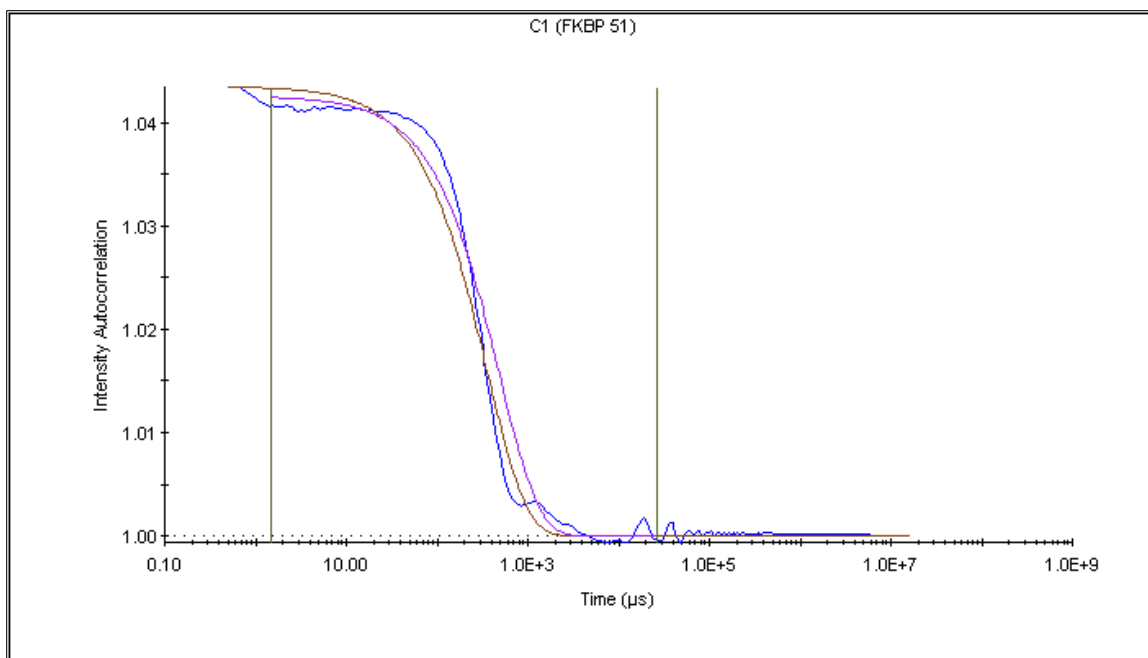
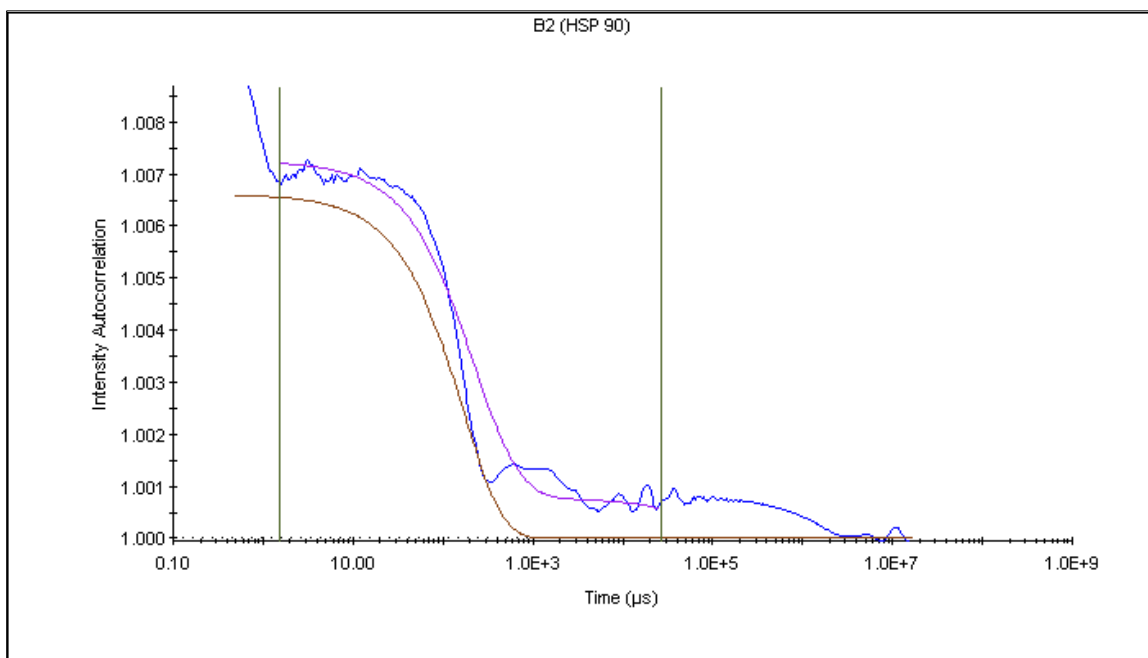


Figure A1. Dynamic Light Scattering Results. Top panel shows DLS of Hsp90 at 0.250 mM and bottom panel shows DLS of FKBP51 at 0.01 mM.

Dynamic Light Scattering

APPENDIX B: NMR Chemical Shift and Assignment Data for FK1

Table A1. Peak List and Chemical Shifts for $^{13}\text{C}^{15}\text{N}$ -labeled FK1

#	AA	C_α	C_β	NH	N
1	M	55.56741	33.16497		
2	T	61.69434	69.7916	8.23567	115.78858
3	T	61.65497	69.82626	8.19406	115.96677
4	D	54.38185	41.24771	8.35551	122.8907
5	E	57.21672	30.05092	8.45057	122.28542
6	G	45.40805		8.41964	109.25886
7	A	52.58298	19.25962	7.9778	123.66524
8	K	56.24578	32.98483	8.18787	120.23803
9	N	53.39845	38.94128		
10	N	53.39845	38.94128	8.38879	119.45626
11	E	56.61387	30.31481	8.29437	120.92284
12	E	56.3829	30.35683	8.32291	121.82581
13	S	55.89612	63.30598	8.39443	117.89005
14	P	63.3929	32.17795		
15	T	61.85286	69.6507	8.16758	114.37888
16	A	52.5358	19.46785	8.22961	126.7705
17	T	61.85162	69.69791	8.05158	113.11143
18	V	62.13806	32.87038	8.15771	122.93578
19	A	52.51447	19.36623	8.35119	127.93896
20	E	56.61197	30.26074	8.34487	120.50468
21	Q	55.9259	29.72264	8.41733	121.23191
22	G	45.53946		8.97852	111.91369
23	E	54.99217	31.74515	8.89347	122.78767
24	D	53.69767	39.86588	8.85458	125.04137
25	I	60.91776	37.459	7.74419	120.21203
26	T	62.50499	70.55043	8.52325	114.17397
27	S	60.52031	62.75695	8.80448	118.17658
28	K	56.96548	32.76416	8.0847	119.48365
29	K	55.10236	32.55208	7.79543	116.817
30	D	52.12553	41.31226	7.69835	117.72147
31	R	57.85491	26.72038		

Continuation of Table A1. Peak List and Chemical Shifts for $^{13}\text{C}^{15}\text{N}$ -labeled FK1

32	G	46.9373		8.87738	105.18037
33	V	62.18152	34.68372	6.2448	115.92564
34	L	52.78006	46.1561	8.4052	125.36332
35	K	54.91516	38.98117	9.12545	121.85793
36	I	59.85765	42.54462	8.9518	125.86557
37	V	64.46331	31.84687	9.10519	128.20941
38	K	54.74797	31.90417	8.74224	128.57001
39	R	55.66148	34.14418	8.10706	121.70131
40	V	62.91138	32.27299	8.49361	126.61909
41	G	44.02576		9.72428	112.99355
42	N	52.85679	41.23154	8.89751	117.45747
43	G	45.40805		8.41274	109.41523
44	E	56.02808	29.46675	8.2779	119.87441
45	E	55.65244	32.84181	8.39538	121.5531
46	T	61.90369	69.72392	8.13522	114.31333
47	P	62.2468	31.5305		
48	M	52.80655	35.19386	8.72412	120.7681
49	I	63.52189	37.10711	8.07589	120.19561
50	G	44.77468		9.33099	116.72478
51	D	55.21166	40.4242	8.42825	123.59737
52	K	55.89235	32.71907	8.8605	122.2594
53	V	59.54971	33.11845	8.63954	119.23489
54	Y	55.81822	39.96127	8.05612	120.81375
55	V	58.32961	35.63976	9.52272	114.98199
56	H	54.73818	35.31664	8.7199	119.20776
57	Y				
58	K	56.2489586	36.5998497	8.95236015	119.182861
59	G	45.5151405		8.98554039	111.861977
60	K	54.8755188	37.53965	9.45153999	124.764107
61	L	54.4146194	42.1315689	8.75926018	120.088226
62	S				
63	N	52.59135	37.42501	7.46643	117.26268

Continuation of Table A1. Peak List and Chemical Shifts for $^{13}\text{C}^{15}\text{N}$ -labeled FK1

64	G	45.02737		8.22791	107.90089
65	K	56.36945	31.47277	8.38256	116.82005
66	K	57.56284	31.01814	8.26131	119.27572
67	F	56.52079	41.14852		
68	D	54.60372	44.47718	6.96678	118.6972
69	S	56.79387	65.20155	8.34758	116.93421
70	S	58.18072	63.72445	8.34475	116.96164
71	H	55.7593	29.46879	8.67103	121.01128
72	D				
73	R				
74	N				
75	E				
76	P	62.54616	32.24281		
77	F	57.77422	41.53698	9.30612	124.91258
78	V	59.28852	34.07311	7.37516	127.25642
79	F	55.50563	40.69008	8.13847	120.83193
80	S	56.62948	63.13042	8.34774	115.3137
81	L	56.59764	42.27339	8.90211	129.84496
82	G	46.86366		9.20708	115.22227
83	K	53.85117	32.762	7.77116	117.24957
84	G	46.6798		8.84247	111.8952
85	Q	56.87688	29.40343	9.23372	118.69217
86	V	57.40725	35.85967	6.82778	109.06683
87	I	61.7086	38.40494	7.07582	111.99664
88	K	59.6177	33.05133	8.88483	124.69365
89	A	55.23829	20.91516	8.8987	114.33505
90	W	59.56803	29.08845	7.61381	115.31712
91	D	57.80404	40.48963	7.06249	121.91173
92	I	63.95063	39.48651	8.12443	115.49307
93	G	47.05078	39.42239	8.48574	105.62881
94	V	66.45195	30.13501	9.3947	124.66789
95	A	53.96693	18.97215	6.33649	116.43687

Continuation of Table A1. Peak List and Chemical Shifts for $^{13}\text{C}^{15}\text{N}$ -labeled FK1

96	T	61.54445	71.13624	7.10846	103.61083
97	M	56.57845	36.2843	7.34722	123.56704
98	K	54.05819	35.12584	7.13474	115.88678
99	K	60.25718	30.50966	9.27812	121.01232
100	G	45.24708	0	9.03284	113.46843
101	E	55.89198	33.88329	8.41961	124.62167
102	I	60.23503	40.25872	8.53228	121.24797
103	C	54.70619	32.6102	9.71229	123.88232
104	H	52.70061	34.74151	9.1962	120.10197
105	L	52.52476	47.22847	9.09416	120.89021
106	L	53.87385	46.24059	9.07495	125.77542
107	C	55.61449	31.3467	9.56105	124.84819
108	K				
109	P	65.60266	31.17132		
110	E	59.57081	28.35925	9.62913	119.00423
111	Y	58.11855	39.41819	8.06457	117.16912
112	A	51.58308	19.36328	7.90091	125.37965
113	Y				
114	G				
115	S				
116	A	54.3014984	19.1370907	8.67115021	124.808411
117	G		44.31707		
118	S	61.2134209	44.2375908	8.60358047	115.618294
119	L				
120	P				
121	K				
122	I				
123	P	61.75363	33.20723		
124	S	59.59579	63.93246	8.3858	113.33275
125	N	54.61055	37.22884	8.16482	120.9895
126	A	52.52291	20.55093	7.94286	121.68728
127	T	63.11993	69.19085	8.60747	122.54504

Continuation of Table A1. Peak List and Chemical Shifts for $^{13}\text{C}^{15}\text{N}$ -labeled FK1

128	L	53.34252	46.44555	8.735	125.40909
129	F	55.4854	42.31112	8.76384	122.74904
130	F	55.94334	44.26237	8.85945	121.27012
131	E	54.88714	32.75718	8.6774	121.46977
132	I	60.20597	41.24478	8.98912	125.79225
133	E	53.24091	33.60151	9.32124	128.84044
134	L	54.34349	40.79915	8.45705	127.92609
135	L	57.07132	42.37034	9.1376	129.53587
136	D	52.82453	42.98111	7.88522	110.93533
137	F	56.57823	42.06094	8.371	115.15088
138	K	57.5233	35.42819	9.11816	124.59063

Table A2. Secondary C α Chemical Shift Values

#	AA	FK1 C α Shift Values (ppm)	Standard C α Shift Values (ppm)	Δ C α (ppm)
1	M	55.56741	55.75	-0.18259
2	T	61.69434	61.87	-0.17566
3	T	61.65497	62.12	-0.46503
4	D	54.38185	54.14	0.24185
5	E	57.21672	56.93	0.28672
6	G	45.40805	45.26	0.14805
7	A	52.58298	52.64	-0.05702
8	K	56.24578	56.67	-0.42422
9	N	53.39845	53.25	0.14845
10	N	53.39845	53.46	-0.06155
11	E	56.61387	56.86	-0.24613
12	E	56.3829	56.46	-0.0771
13	S	55.89612	56.75	-0.85388
14	P	63.3929	63.78	-0.3871
15	T	61.85286	61.84	0.01286
16	A	52.5358	52.85	-0.3142
17	T	61.85162	61.83	0.02162
18	V	62.13806	62.55	-0.41194
19	A	52.51447	52.68	-0.16553
20	E	56.61197	56.71	-0.09803
21	Q	55.9259	56.25	-0.3241
22	G	45.53946	45.34	0.19946
23	E	54.99217	56.64	-1.64783
24	D	53.69767	53.94	-0.24233
25	I	60.91776	61.82	-0.90224
26	T	62.50499	61.89	0.61499
27	S	60.52031	58.72	1.80031
28	K	56.96548	56.69	0.27548
29	K	55.10236	56.68	-1.57764
30	D	52.12553	54.03	-1.90447
31	R	57.85491	56.7	1.15491

Continuation of Table A2. Secondary Ca Chemical Shift Values

32	G	46.9373	45.16	1.7773
33	V	62.18152	62.51	-0.32848
34	L	52.78006	55.3	-2.51994
35	K	54.91516	56.47	-1.55484
36	I	59.85765	61.38	-1.52235
37	V	64.46331	62.5	1.96331
38	K	54.74797	56.56	-1.81203
39	R	55.66148	56.28	-0.61852
40	V	62.91138	62.55	0.36138
41	G	44.02576	45.37	-1.34424
42	N	52.85679	53.3	-0.44321
43	G	45.40805	45.54	-0.13195
44	E	56.02808	56.62	-0.59192
45	E	55.65244	56.49	-0.83756
46	T	61.90369	60.06	1.84369
47	P	62.2468	63.86	-1.6132
48	M	52.80655	55.62	-2.81345
49	I	63.52189	61.55	1.97189
50	G	44.77468	45.39	-0.61532
51	D	55.21166	53.94	1.27166
52	K	55.89235	56.67	-0.77765
53	V	59.54971	62.28	-2.73029
54	Y	55.81822	58.04	-2.22178
55	V	58.32961	62.51	-4.18039
56	H	54.73818	55.14	-0.40182
57	Y		58.22	
58	K	56.24895859	56.76	-0.5110414
59	G	45.51514053	45.25	0.2651405
60	K	54.8755188	56.62	-1.7444812
61	L	54.41461945	55.34	-0.9253806
62	S		58.72	
63	N	52.59135	53.44	-0.84865
64	G	45.02737	45.51	-0.48263

Continuation of Table A2. Secondary Ca Chemical Shift Values

65	K	56.36945	56.53	-0.16055
66	K	57.56284	56.42	1.14284
67	F	56.52079	58.1	-1.57921
68	D	54.60372	54.1	0.50372
69	S	56.79387	58.83	-2.03613
70	S	58.18072	58.7	-0.51928
71	H	55.7593	55.53	0.2293
72	D		53.99	
73	R		56.72	
74	N		52.98	
75	E		54.88	
76	P	62.54616	63.46	-0.91384
77	F	57.77422	57.85	-0.07578
78	V	59.28852	62.47	-3.18148
79	F	55.50563	58	-2.49437
80	S	56.62948	58.67	-2.04052
81	L	56.59764	55.63	0.96764
82	G	46.86366	45.32	1.54366
83	K	53.85117	56.7	-2.84883
84	G	46.6798	45.25	1.4298
85	Q	56.87688	55.94	0.93688
86	V	57.40725	62.43	-5.02275
87	I	61.7086	61.46	0.2486
88	K	59.6177	56.51	3.1077
89	A	55.23829	52.6	2.63829
90	W	59.56803	57.61	1.95803
91	D	57.80404	53.94	3.86404
92	I	63.95063	61.7	2.25063
93	G	47.05078	45.15	1.90078
94	V	66.45195	62.44	4.01195
95	A	53.96693	52.74	1.22693
96	T	61.54445	62.16	-0.61555
97	M	56.57845	55.81	0.76845

Continuation of Table A2. Secondary Ca Chemical Shift Values

98	K	54.05819	56.53	-2.47181
99	K	60.25718	56.68	3.57718
100	G	45.24708	45.25	-0.00292
101	E	55.89198	56.49	-0.59802
102	I	60.23503	61.53	-1.29497
103	C	54.70619	58.5	-3.79381
104	H	52.70061	55.41	-2.70939
105	L	52.52476	55.38	-2.85524
106	L	53.87385	55.46	-1.58615
107	C	55.61449	58.32	-2.70551
108	K		54.81	
109	P	65.60266	63.52	2.08266
110	E	59.57081	56.5	3.07081
111	Y	58.11855	58.15	-0.03145
112	A	51.58308	52.65	-1.06692
113	Y		58.35	
114	G	46.39273	45.37	1.02273
115	S		58.52	
116	A	54.3014984	52.93	1.3714984
117	G		45.37	
118	S	61.2134209	58.39	2.8234209
119	L		53.62	
120	P		63.55	
121	K		56.32	
122	I		59.62	
123	P	61.75363	63.57	-1.81637
124	S	59.59579	58.69	0.90579
125	N	54.61055	53.29	1.32055
126	A	52.52291	52.98	-0.45709
127	T	63.11993	61.9	1.21993
128	L	53.34252	55.33	-1.98748
129	F	55.4854	57.89	-2.4046
130	F	55.94334	58.03	-2.08666

Continuation of Table A2. Secondary C α Chemical Shift Values

131	E	54.88714	56.56	-1.67286
132	I	60.20597	61.57	-1.36403
133	E	53.24091	56.59	-3.34909
134	L	54.34349	55.44	-1.09651
135	L	57.07132	55.47	1.60132
136	D	52.82453	53.91	-1.08547
137	F	56.57823	58.26	-1.68177
138	K	57.5233	56.75	0.7733
139	G	45.38262	45.25	0.13262
140	K	58.0316	57.89	0.1416

Table A3. Intensity Ratios for free FK1 vs. FK1 in the presence of tau

AA	FK1 Intensity	FK1+tau Intensity	FK1+tau Intensity Ratio
2T	2.0815506	1.571737885	0.755080317
3T	2.2140162	1.856165528	0.838370347
4D	2.29990005	1.817488194	0.790246598
5E	0.23636067	0.163030565	0.689753356
6G	2.64907932	2.136030912	0.80632954
7A	3.46071339	2.756175041	0.796418175
8K	2.29751134	1.922115684	0.836607703
9N	1.69227874	1.360085607	0.803700698
10N	1.63955057	1.3586905	0.828696917
11E	2.03474689	1.744387507	0.85729951
12E	2.29641366	1.748647332	0.76146879
13S	1.94202912	1.545189261	0.795657103
15T	0.80534911	0.587622881	0.729649878
16A	0.94885361	0.632546067	0.666642419
17T	1.20860803	0.953160942	0.788643561
18V	0.68527681	0.513116896	0.748773184
19A	0.84457272	0.600877225	0.711457059
20E	1.00974154	0.712035418	0.705166011
21Q	0.50692153	0.424958646	0.838312483
22G	0.66873491	0.474486232	0.709528134
23E	0.58808452	0.412037343	0.70064307
24D	0.71550715	0.522549987	0.730321125
25I	0.39698616	0.275571555	0.694159104
26T	0.61310589	0.445648968	0.726871122
27S	0.17445417	0.151075348	0.86598876
28K	0.47302878	0.367112964	0.776090125
29K	0.3725163	0.23927182	0.642312341
30D	0.50862378	0.368313879	0.724138143
31R	0.52281934	0.340140849	0.650589646
32G	0.62486017	0.44931066	0.719057933
33V	0.93226594	0.664797068	0.713098099
34L	0.54730803	0.384274095	0.70211668
35K	0.47936392	0.326564342	0.681245144
36I	0.48633564	0.36034897	0.740947082
37V	0.57292295	0.492393255	0.859440627
38K	0.26631987	0.184845909	0.694074794

Continuation of Table A3. Intensity Ratios for free FK1 vs. FK1 in the presence of tau

39R	0.55344117	0.382978946	0.691995769
40V	0.7088778	0.519112289	0.732301516
41G	0.35309327	0.262744933	0.744123319
42N	0.80480903	0.599369824	0.744735457
43G	1.41017783	1.063755393	0.754341313
44E	0.8486591	0.626165867	0.737829675
45E	1.44434094	1.153669477	0.798751487
46T	0.93181455	0.6712479	0.720366406
48M	0.60378766	0.464031279	0.768533889
49I	0.89523274	0.745827019	0.833109635
50G	0.45728692	0.30643028	0.670105057
51D	0.75708067	0.507020235	0.669704369
52K	0.61306554	0.455993474	0.743792373
53V	0.47642744	0.329911619	0.692469817
54Y	0.41486186	0.356076956	0.858302466
55V	0.54645205	0.407720923	0.746123886
56H	0.36993194	0.24526237	0.662993231
58K	0.44404504	0.290670931	0.654597861
59G	0.39633289	0.304258168	0.767683368
60K	0.22281384	0.156543091	0.702573447
61L	0.39752051	0.264596671	0.665617654
62S	0.35685569	0.276965499	0.776127455
63N	0.54194355	0.41367808	0.763323191
64G	0.57526714	0.443878949	0.771604913
65K	0.86597055	0.677552223	0.782419473
68D	0.16404828	0.090796247	0.553472702
69S	0.55121118	0.38378647	0.696260317
77F	0.36279431	0.259303302	0.714739164
78V	0.7041921	0.502064824	0.712965713
79F	0.58606732	0.476261199	0.812639066
80S	0.61227983	0.475717515	0.776960941
81L	0.52750337	0.340540469	0.645570222
82G	0.33563405	0.239697993	0.714164701
83K	0.5111787	0.383677781	0.749682549
84G	0.65550792	0.492196769	0.750863188
85Q	0.47882631	0.338927388	0.707829495
86V	0.79716527	0.590089977	0.740235426

Continuation of Table A3. Intensity Ratios for free FK1 vs. FK1 in the presence of tau

87I	0.51127338	0.349425405	0.683441415
88K	0.47088343	0.356784374	0.757691504
89A	0.62463862	0.481520832	0.770879063
90W	0.56601131	0.406965405	0.719005783
91D	0.53528047	0.398370355	0.744227336
92I	0.73629087	0.514921367	0.699345037
93G	0.57586193	0.425936848	0.739650991
94V	0.68403339	0.489171654	0.715128323
95A	0.98531425	0.70143038	0.711884945
96T	0.55311465	0.377688617	0.682839651
97M	0.5972985	0.431293696	0.722073961
98K	0.48438108	0.346046567	0.714409752
99K	0.58455163	0.421291023	0.720707975
100G	0.4949806	0.344621211	0.696231749
101E	0.49696141	0.349454761	0.703182883
102I	0.36563209	0.253906608	0.694431962
103C	0.41093639	0.292154461	0.710948146
104H	0.34284437	0.281994373	0.822514236
105L	0.44519448	0.339602709	0.762818772
106L	0.50184929	0.341067404	0.679621169
107C	0.4289239	0.329630345	0.768505419
110E	0.38721669	0.284746468	0.735367244
111Y	0.43084106	0.37682122	0.87461771
112A	0.5588764	0.411809951	0.736853363
114G	0.25532582	0.194436908	0.761524646
116A	0.44393265	0.355948061	0.801806442
117G	0.02279598	0.017281402	0.758089861
118S	0.16000305	0.115745857	0.723397813
119L	0.02980269	0.019768994	0.663329083
124S	0.49843192	0.369672626	0.741671251
125N	0.41128477	0.268492132	0.652813206
126A	0.35575125	0.254295707	0.714813256
127T	0.22993352	0.165530533	0.719906067
128L	0.37319833	0.265930682	0.712572005
129F	0.30564055	0.216774046	0.709245051
130F	0.47152317	0.349685639	0.741608609
131E	0.38129213	0.302467048	0.793268522

Continuation of Table A3. Intensity Ratios for free FK1 vs. FK1 in the presence of tau

132I	0.46471131	0.322362423	0.69368319
133E	0.29698965	0.22830756	0.768739114
134L	0.39588371	0.310977191	0.785526617
135L	0.35332963	0.223280892	0.631933678
136D	0.66940665	0.496039331	0.741013447
137F	0.8076756	0.660482466	0.817757112
138K	0.59618878	0.446191072	0.748405681
139G	1.01781547	0.755611837	0.742385883
140E	2.83270001	2.035108089	0.718434031

APPENDIX C: NMR Chemical Shift and Assignment Data for tau

Table A4. Intensity Ratios for ¹⁵N-labeled tau titrations

AA	Tau + 90 Intensity Ratio	Tau + 51 Intensity Ratio	Tau + 90 + 51 Intensity Ratio
1M			
2A			
E3			
P4			
R5	0.563655183	0.658731332	0.578663315
Q6	0.460157933	0.62479062	0.60720268
E7			
F8			
E9	0.291696578	0.647284039	0.496290979
V10	0.583167132	0.542879936	0.389409653
M11	0.574611611	0.588307441	0.44215045
E12	0.47552297	0.505022726	0.331411172
D13	0.595349033	0.537663304	0.388995034
H14	0.463674434	0.532568351	0.342138174
A15	0.498193206	0.658395567	0.373006504
G16	0.519802432	0.508132211	0.366479352
T17	0.538627593	0.641875652	0.510737134
Y18	0.449016709	0.610605685	0.462978607
G19	0.559082247	0.658529285	0.585855579
I20			
G21	0.436700242	0.748491356	0.663125374
D22	0.567556003	0.670443083	0.577604213
R23	0.487961528	0.651487585	0.49052282
K24			
D25	0.553988476	0.64829619	0.560346019
Q26	0.512058185	0.693982329	0.551521772
G27	0.536147707	0.581583296	0.406375753
G28	0.572536794	0.690698879	0.591074938
Y29			
T30	0.562178578	0.668818424	0.572901925
M31			
H32	0.534912026	0.668999808	0.576730586
Q33			
D34	0.530210685	0.632132948	0.54895138

Continuation of Table A4. Intensity Ratios for ¹⁵N-labeld tau titrations

Q35			
E36	0.56364554	0.658786223	0.578682047
G37	0.540518319	0.676012667	0.593583025
D38	0.52366567	0.64614455	0.59703198
T39	0.513005671	0.678593364	0.568288174
D40			
A41			
G42	0.567761874	0.673543812	0.597310808
L43	0.560018347	0.665717163	0.585296816
K44			
A103			
E104	0.445088355	0.644056151	0.487154614
E105			
A106			
G107	0.558889922	0.689501639	0.586248248
I108	0.551368495	0.665175776	0.583784665
G109	0.551876396	0.671613043	0.605936084
D110	0.424753442	0.477912312	0.448711492
T111	0.537138882	0.649388098	0.577753558
112			
S113	0.549744388	0.68852623	0.586210755
L114	0.578371186	0.662977863	0.492820283
E115	0.448774455	0.625536309	0.445700906
D116			
E117			
A118	0.349745502	0.625004721	0.424296242
A119	0.541917558	0.662962808	0.578893661
G120	0.56703789	0.694277866	0.604295003
H121			
V122			
T123			
Q124			
A125			
R126			
M127	0.504458289	0.625181246	0.553374481
V128			
S129	0.603656197	0.696015845	0.623544032
K130	0.565956343	0.676893695	0.610068356

Continuation of Table A4. Intensity Ratios for ¹⁵N-labeld tau titrations

S131	0.590029427	0.693342049	0.600704728
K132	0.603616256	0.708629606	0.634291229
D133	0.566055642	0.674855496	0.615224031
G134	0.566535492	0.665288394	0.583902619
T135	0.57423332	0.665499696	0.58816399
G136	0.568181145	0.678885199	0.606178923
S137	0.529434625	0.689675957	0.582795056
D138	0.551656676	0.632037219	0.54518723
D139			
K140	0.568476419	0.680863606	0.580947308
K141			
A142	0.598062499	0.677845765	0.607356845
K143	0.422647515	0.629791068	0.469616902
G144	0.556534877	0.685344863	0.590757039
A145	0.349431399	0.60563214	0.521752135
D146	0.576517668	0.691794682	0.601718829
G147	0.5922303	0.67276471	0.609747113
K148	0.539992028	0.658482508	0.507697111
T149			
K150	0.550540323	0.718219686	0.589699113
I151			
A152	0.509092584	0.664094622	0.562504076
T153	0.487434198	0.653958932	0.568438558
P154			
R155	0.551594266	0.662633334	0.589034823
G156	0.511503776	0.671057017	0.546000099
A157	0.577101028	0.675945741	0.592793668
A158	0.537443178	0.667139641	0.55807586
P159			
P160			
G161	0.553195112	0.681041828	0.605174983
Q162			
K163	0.507109564	0.6504144	0.563726664
G164	0.506787813	0.66799362	0.56275482
Q165			
A166	0.605322565	0.727961696	0.62627316
N167	0.594227721	0.706589746	0.618050969
A168			

Continuation of Table A4. Intensity Ratios for ¹⁵N-labeld tau titrations

T169	0.566722283	0.66140803	0.572126938
R170	0.597489209	0.710107383	0.61710168
I171	0.482639524	0.663946012	0.532088793
P172			
A173	0.509800668	0.657918441	0.536828667
K174	0.395378692	0.628769507	0.426913917
T175	0.570705621	0.628422873	0.544523096
P176			
P177			
A178	0.413361394	0.642921182	0.446280626
P179			
K180			
T181	0.612909756	0.699943911	0.59927901
P182			
P183			
S184			
S185	0.594227721	0.706589746	0.618050969
G186	0.544894423	0.613984487	0.484690421
E187	0.414693092	0.623085602	0.478537691
P188			
P189			
K190	0.476678925	0.569112311	0.475700468
S191	0.556191116	0.679428203	0.588657044
G192	0.62370398	0.743249153	0.680065286
D193			
R194	0.518990504	0.663443077	0.561588812
S195	0.557333958	0.701110151	0.588434201
G196	0.550528837	0.736893123	0.566782599
Y197			
S198	0.544368672	0.677999565	0.560565635
S199	0.457921878	0.637167342	0.520607072
P200			
G201	0.570129462	0.75956661	0.6388008
S202	0.516120201	0.635255902	0.530996708
P203			
G204	0.552789084	0.724999522	0.599358228
T205	0.530481576	0.671387238	0.565259229
P206			

Continuation of Table A4. Intensity Ratios for ¹⁵N-labeld tau titrations

G207	0.545350495	0.687574623	0.610548883
S208	0.527429056	0.641822794	0.563684105
R209			
S210	0.563634131	0.711116306	0.612867112
R211			
T212	0.415590361	0.596324992	0.43763959
P213			
S214	0.482848234	0.645150218	0.518390128
L215	0.452609778	0.626211309	0.498394316
P216			
T217			
P218			
P219			
T220	0.566649832	0.681633559	0.619838898
R221	0.40647401	0.61474607	0.499717459
E222	0.454145141	0.667921287	0.504390029
P223			
K224			
K225			
V226	0.346086361	0.604781649	0.40628609
A227	0.359948081	0.598244408	0.408461516
V228	0.355216062	0.565082854	0.376813031
V229			
R230	0.401542827	0.604954645	0.398035655
T231			
P232			
P233			
K234			
S235	0.447297223	0.615558512	0.443244808
P236			
S237	0.522586604	0.657102734	0.571724571
S238	0.445098455	0.648321167	0.449158192
A239	0.459908207	0.626949161	0.482924848
K240			
S241	0.485981005	0.650589499	0.529372205
R242			
L243	0.429900947	0.639063778	0.449124618
Q244			

Continuation of Table A4. Intensity Ratios for ¹⁵N-labeld tau titrations

T245	0.453201279	0.626363001	0.479075647
A246	0.469928561	0.629553852	0.514396308
P247			
V248			
P249			
M250	0.411257788	0.607036898	0.446195771
P251			
D252	0.324657967	0.599545518	0.403455394
L253			
K254			
N255	0.411642211	0.591885646	0.454633287
V256	0.443612455	0.621998509	0.464536248
K257	0.524446213	0.610280502	0.521093484
S258			
K259			
I260	0.502893749	0.65440416	0.539792697
G261	0.425336919	0.609169162	0.494913644
S262	0.541750439	0.650972989	0.562556083
T263	0.522765395	0.673376015	0.590245693
E264			
N265			
L266	0.508323477	0.657839414	0.525154101
K267			
H268			
Q269			
P270			
G271	0.543593373	0.659608234	0.558650108
G272			
G273	0.533698415	0.68950265	0.664419406
K274	0.552813175	0.642916019	0.557096169
V275	0.328242716	0.303893994	0.179598568
Q276	0.232490192	0.554065555	0.2944053
I277	0.166476233	0.298956991	0.190141179
I278	0.149322538	0.285999852	0.187642473
N279	0.296233689	0.599237798	0.350953245
K280	0.501265277	0.522646135	0.33260292
K281	0.533697923	0.682775483	0.601790718
L282	0.354495834	0.633083251	0.400653602

Continuation of Table A4. Intensity Ratios for ¹⁵N-labeld tau titrations

D283	0.615849087	0.663583209	0.570223714
L284	0.531738081	0.703859892	0.532063571
S285	0.403026007	0.608751058	0.435794052
N286	0.500440509	0.676943173	0.548128063
V287	0.350227351	0.57827035	0.390243163
Q288	0.464021612	0.614337205	0.512778453
S289	0.556191116	0.679428203	0.588657044
K290	0.529195452	0.670828456	0.565762485
C291	0.544341454	0.664913065	0.560007275
G292	0.610744855	0.738800491	0.609777696
S293	0.523254302	0.632495159	0.544273357
K294	0.538924143	0.66977247	0.584696434
D295			
N296	0.404845368	0.651322665	0.432691177
I297	0.335505195	0.63021978	0.493269806
K298	0.425620885	0.679372784	0.541556199
H299	0.532065483	0.658212085	0.537649048
V300	0.499885122	0.672829256	0.528301762
P301			
G302	0.47320917	0.645367435	0.51044059
G303			
G304			
S305	0.538926479	0.662941725	0.555327943
V306	0.428650504	0.634195242	0.437174349
Q307	0.383467356	0.601611936	0.43335407
I308	0.188096108	0.532463285	0.203248975
V309	0.146717661	0.528840905	0.181544525
Y310	0.160285407	0.563115243	0.217823265
K311	0.163175808	0.543293711	0.197567621
P312			
V313	0.151091477	0.541326913	0.183414719
D314	0.203608125	0.570160133	0.25248624
L315			
S316	0.267749485	0.526825628	0.29980627
K317	0.298531162	0.569336575	0.293421162
V318	0.330999239	0.5608154	0.33546162
T319	0.420713892	0.631633207	0.452067545
S320	0.414710682	0.63656025	0.448679157

Continuation of Table A4. Intensity Ratios for ¹⁵N-labeld tau titrations

K321			
C322	0.467519529	0.660275481	0.531378483
G323	0.489275924	0.640349697	0.475143965
S324	0.388179152	0.504397611	0.399054019
L325	0.458781294	0.63038341	0.483641494
G326	0.491461765	0.653021784	0.509876051
N327	0.518571356	0.654046664	0.535676125
I328	0.598809443	0.697776557	0.609396097
H329			
H330	0.564693244	0.426873664	0.380315951
K331	0.60904554	0.641128443	0.478119992
P332			
G333	0.392590567	0.630739536	0.445482845
G334			
G335			
Q336	0.546936142	0.661146792	0.477218683
V337			
E338	0.44585054	0.64159492	0.491862908
E339	0.448919849	0.633266318	0.481675293
K340	0.493528207	0.660870962	0.509104723
S341	0.456663737	0.661584532	0.48936215
E342	0.453296573	0.638764547	0.49071746
K343	0.428801154	0.57739353	0.448345414
L344	0.507322395	0.655779485	0.53710633
D345	0.535519344	0.658283005	0.558377344
F446	0.471041939	0.663040233	0.518455501
K347	0.416857139	0.618689679	0.474791039
D348			
R349	0.321223414	0.527280974	0.342991499
V350	0.399370727	0.567926277	0.388698787
Q351	0.365010646	0.569632043	0.387227139
S352	0.446566923	0.595543186	0.44790599
K353	0.449156455	0.572022195	0.453492793
I354	0.351530256	0.562181365	0.361210785
G355	0.49132283	0.615320429	0.475280613
S356	0.475671815	0.639146465	0.515519549
L357	0.424267449	0.604638394	0.449275441
D358	0.43273195	0.549341142	0.41237699

Continuation of Table A4. Intensity Ratios for ¹⁵N-labeld tau titrations

N359	0.504613582	0.640518412	0.535242631
I360	0.361139253	0.580864999	0.398868583
T361	0.515218207	0.667185972	0.550807169
H362			
V363	0.406689718	0.558753961	0.465253255
P364			
G365	0.412679947	0.655986541	0.539037108
G366			
G367			
N368	0.567335505	0.72388699	0.617084665
K369	0.507695885	0.659890078	0.542653219
K370	0.491763689	0.651592485	0.529374545
I371	0.490938496	0.603960977	0.498559205
E372	0.378705754	0.630622456	0.45028864
T373			
H374			
K375	0.504265979	0.671113396	0.540766243
L376	0.448919849	0.633266318	0.481675293
T377	0.363676437	0.606673997	0.391807232
F378			
R379	0.413351769	0.625096872	0.460747293
E380	0.535864867	0.628196487	0.544263814
N381	0.450502428	0.639920175	0.482877291
A382	0.569392179	0.672179852	0.576140417
K383			
A384	0.40980873	0.637745344	0.470418426
K385	0.462514678	0.686147896	0.551762933
T386	0.450773072	0.62670671	0.434457193
D387			
H388			
G389	0.634786782	0.724364809	0.639258417
A390	0.512951935	0.668398442	0.534282064
E391			
I392	0.364842462	0.616658732	0.391910891
V393	0.509978002	0.645306464	0.56601639
Y394	0.413744802	0.627735012	0.423195452
K395	0.438448266	0.654688033	0.472225107
S396			

Continuation of Table A4. Intensity Ratios for ¹⁵N-labeld tau titrations

P397	0.344966644	0.663184431	0.706295335
V398	0.430171004	0.636208595	0.461482216
V399	0.551851519	0.683704991	0.596380141
S400			
G401			
D402	0.530700928	0.656275842	0.568277706
T403			
S404	0.563520086	0.701563194	0.56575212
P405			
R406	0.4514698	0.592643755	0.428245951
H407			
L408			
S409	0.485864546	0.668404577	0.542346318
N410	0.517918988	0.610497553	0.568670044
V411	0.460781816	0.624058255	0.44894193
S412			
S413	0.578292195	0.674343973	0.562925046
T414	0.549572028	0.677406373	0.563870896
G415	0.511127688	0.682041939	0.547359624
S416	0.531782543	0.685823594	0.568646242
I417			
D418			
M419			
V420	0.495895998	0.662465563	0.562302699
D421	0.539203845	0.637229433	0.54066344
S422	0.499960853	0.664395663	0.520364219
P423			
Q424	0.473870296	0.636294572	0.490784143
I425			
A426	0.564700954	0.682193855	0.602583863
T427	0.438093782	0.630953658	0.441377421
L428	0.384770812	0.63494548	0.397617852
A429	0.426516113	0.623821569	0.458194268
D430	0.403850998	0.62479308	0.424794774
E431	0.358545494	0.565444167	0.394454207
V432	0.3876424	0.630789588	0.42022285
S433	0.488222259	0.619148747	0.531440583
A434	0.417916758	0.652867025	0.419805706

Continuation of Table A4. Intensity Ratios for ¹⁵N-labeled tau titrations

S435			
L436	0.43366129	0.616457457	0.429287907
437	0.453728278	0.624593377	0.433832448
K438			
Q439			
G440	0.503750436	0.628980282	0.480989264
L441	0.4553879	0.611834579	0.446429996

Table A5. Intensity Ratio Plot Averages and Standard Deviation Values

AVERAGES	tau + Hsp90		
	(270-441)	(1-40)	(1-441)
MEAN	0.45145733	0.51880157	0.48144882
STDEV	0.10274495	0.06254841	0.0924332
AVERAGES	tau + FKBP51		
	(270-441)	(1-40)	(1-441)
MEAN	0.6328808	0.62887167	0.64189832
STDEV	0.04992598	0.06128861	0.04977791
AVERAGES	tau + Hsp90 + FKBP51		
	(270-441)	(1-40)	(1-441)
MEAN	0.47757278	0.51885178	0.50760078
STDEV	0.10098332	0.11848967	0.09631686

APPENDIX D: Full length Intensity Ratio Plots for tau titrations

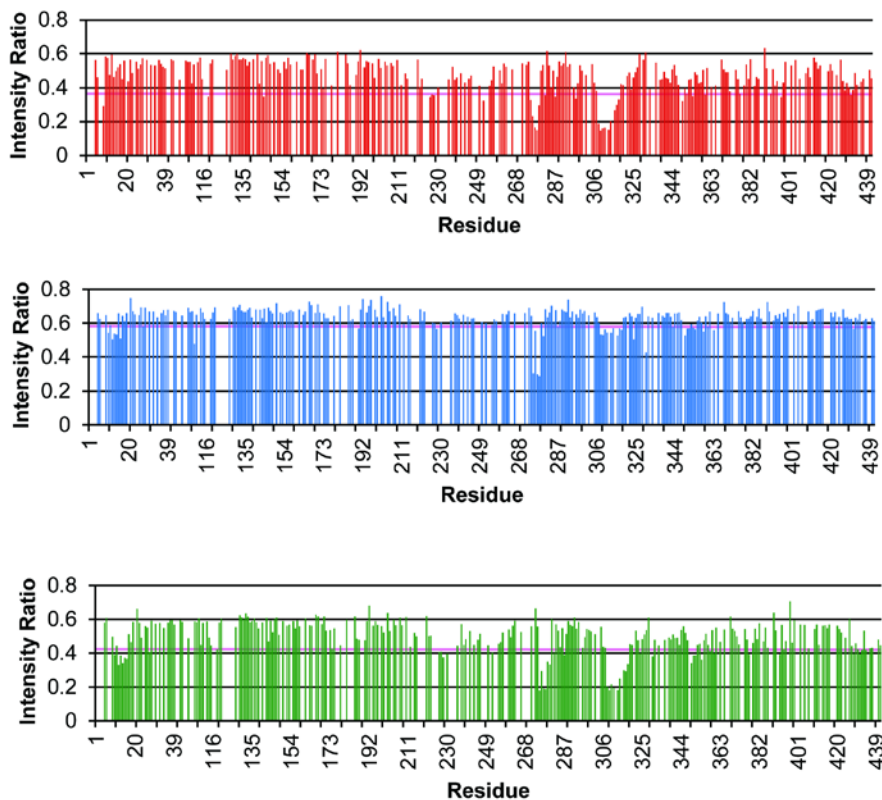


Figure A2: Full length Intensity Ratio Plots for tau titrations. Intensity ratio plots for ^{15}N -labeled tau in the presence of Hsp90 and/or FKBP51. The two regions that experience the largest reductions are two hydrophobic hexapeptide regions, V275 – K280 and V306 – K311. Some residues in the N-terminus also undergo significant reductions. The pink line on each plot indicates one standard deviation below the mean and was calculated from the average intensity ratios for all assigned residues.